Brigham Young University
BYU ScholarsArchive

2011-08-08

Scaling Carbon Nanotube Localization by Floating Potential Dielectrophoresis: An Enabling Geometry

Brian S. Davis
Brigham Young University - Provo

www.manaraa.com

Scaling Parallel Dielectrophoresis of Carbon Nanotubes: an Enabling Geometry

Brian Scott Davis

A thesis submitted to the faculty of
Brigham Young University
in partial fulfillment of the requirements for the degree of

Master of Science

Robert C. Davis, Chair
John N. Harb
R. Steven Turley

Department of Physics and Astronomy

Brigham Young University

December 2011

ABSTRACT

Scaling Parallel Dielectrophoresis of Carbon Nanotubes: an Enabling Geometry

Brian Scott Davis
Department of Physics and Astronomy
Master of Science

Dielectrophoresis has been used as a technique for the parallel localization and alignment of both semiconducting and metallic carbon nanotubes (CNTs) at junctions between electrodes. A variation of this technique known as Floating Potential Dielectrophoresis (FPD) allows for a self-limiting number of CNTs to be localized at each junction, on a massively parallel scale. However, the smallest FPD geometries to date are restricted to conductive substrates and have a lower limit on floating electrode size. We present a geometry which eliminates this lower limit and enables FPD to be performed on non-conducting substrates. We also discuss experiments clarifying the self-limiting mechanism of CNT localization and how it can be used advantageously as devices are scaled downward to smaller sizes.

Keywords: Carbon Nanotube, Dielectrophoresis

ACKNOWLEDGMENTS

Contents

Chapter 1

Introduction

1.1 Carbon Nanotubes

Carbon nanotubes (CNTs) can be viewed as derivatives of graphene, which is a one-atom-thick sheet of carbon atoms arranged in a hexagonal lattice. Graphene's lattice structure allows the carbon atoms to form sp^2 hybridized orbitals, which leaves a pair of pi electrons per carbon atom free to conduct. While graphene thus exhibits metallic behavior, rolling graphene sheets into CNTs imposes periodic boundary conditions on the lattice, creating the possibility of a band gap. In short, CNTs can range from metals to semiconductors, depending on the direction the graphene is rolled up. The "twistiness" of the CNT is more formally defined as its chirality, and so the electrical properties of CNTs are said to be highly chirality-dependent.

While illustrations of rolled graphene help us to understand the electrical properties of CNTs, nanotubes aren't really created by rolling graphene up. A Japanese physicist named Sumio Iijima is usually credited as the first to develop a controllable method of fabricating CNTs, using arc-discharge evaporation [1]. Additionally, CNTs can be grown from metal catalysts using chemical vapor deposition (CVD) [2] or blasted from hunks of graphite using high-energy laser pulses in a
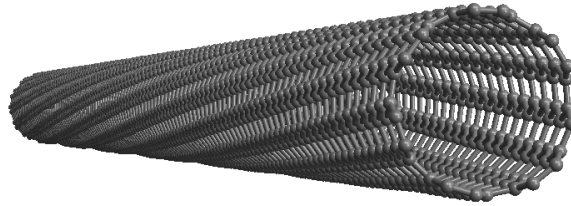
Figure 1.1 A single-walled carbon nanotube. Rendered in Mathematica from coordinate data produced with TubeVBS.

technique known as laser ablation [3]. In all three of these methods the CNTs come as a random mixture of chiralities, and thus a mix of semiconducting and metallic behavior. This fact was first predicted theoretically in 1992 by John Mintmire's group at the Naval Research Laboratory [4] and experimentally confirmed in the labs of Cees Dekker [5] and Charles Lieber [6] in 1998 by correlating atomically-resolved STM images of tubes to transport properties.

Regardless of their electronic type, however, CNTs are good conductors. Metallic tubes have higher conductivity than copper and silver, the best bulk conductors we know of to date. Semiconducting tubes have electron mobilities [7] more than an order of magnitude better than silicon and when configured as transistors have extremely high on-off state current ratios ($\geq 10^8$) [8]. Due to these excellent electronic properties, single-walled CNTs have been used to make molecular-scale field effect transistors (FET) [9], which in turn have been used to fabricate circuits [10, 11], chemical sensors [12], and even a transistor radio [13].

However, a common characteristic of these initial electrical studies was that the CNT devices were made with "brute force" fabrication methods: CNTs randomly dispersed or transferred onto a substrate were located in relation to alignment marks using microscopy techniques and subsequently wired up to create an ad-hoc device [14]. Such methods enabled data to be taken to confirm theoretical understanding of CNT electrical properties, but at the steep cost of many man-hours per device [15]. Other methods have been developed that are less time-intensive [16], but in all cases

these methods are not scalable to studies involving many-CNT devices or commercial operations. In general, the challenge of controlled alignment and precise placement, as well as the confirmed fact that as-grown CNTs come as a mixture of semiconducting and metallic tubes, has prevented the use of CNTs in large-scale electronics.

1.2 Dielectrophoresis

Dielectrophoresis (DEP), first developed in 1951 [17], offers a possible solution to these challenges. A concatenation of the word "dipole" with the word "electrophoresis," dielectrophoresis is defined as the translational motion of neutral matter caused by polarization effects in a nonuniform electric field. Similar to electrophoresis, where matter moves through a viscous gel at a rate dependent on its charge and the applied DC electric field, in dielectrophoresis, dipoles are induced in matter by an AC electric field, which causes movement at a rate dependent on relative polarizability. One can view DEP transport as a phenomenon similar to shaking a bowl full of sand and marbles, but with polarizability density rather than mass density being the agent for one species giving way to the other.

DEP was first applied to CNT localization in 1998 [18]. Because DEP is a solution-based localization technique, it can be used in conjunction with other solution-based techniques that purify CNTs to a single electronic type after growth [19, 20]. While this alone makes DEP a good candidate for electronic CNT device applications, dielectrophoretically placed CNTs are able to survive standard process steps used in photolithography [21], the primary micro- and nanoscale fabrication technique used today, and have already been successfully incorporated as interconnect wires into GHz resonators [22]. Much work in developing DEP has been done with this intent in mind [23, 24].

However, the first few attempts of performing DEP by directly driving the electrodes did not

produce pristine results [18, 23, 25–28]. Many carbon particles and other solution impurities were localized with the CNTs, and a random number of CNTs were localized between each pair of electrodes. While it was soon found that localized contamination could be partially avoided by improved solution preparation and the use of high-frequency AC driving signals [25], many potential applications of CNT devices require a large array of electrode pairs with a controlled number of CNTs at each junction.

One method exhibiting self-limiting localization is to put a large resistor in series with the driving signal that effectively shuts off the voltage once a tube is localized [23, 28, 29]. In the words of those who first pioneered the technique, "the series resistance is expected to act as a voltage divider and current limiter. As soon as a contact is formed between the electrodes via a nanotube and the resulting resistance is smaller than the series resistance, the applied voltage will mainly drop along the latter. Hence the field between the electrodes will collapse and the trapping of additional tubes will be automatically prevented." [29] Three years later an important extension of this work was performed by Banerjee et al. in which the number of captured CNTs was studied as a function of the magnitude of the series resistor [28]. When very large resistors were used, devices attracted single tubes, and as resistors of less magnitude were used larger numbers of CNTs were localized. In spite of the precision and control that has been developed using this method, there is an obvious challenge in scaling due to the necessity for DEP to be performed serially on each junction.

Self-limiting CNT localization has also been observed in experiments involving a technique called Floating Potential Dielectrophoresis (FPD), in which CNTs are localized between electrode(s) left at floating potential rather than electrodes that are directly driven [27, 30]. In contrast to the limiting resistor method just discussed, FPD has recently been demonstrated as a parallelizable technique capable of yields greater than 90% and high device densities [24]. Two main FPD geometries have been developed in the literature and are described in detail in figure 1.2.
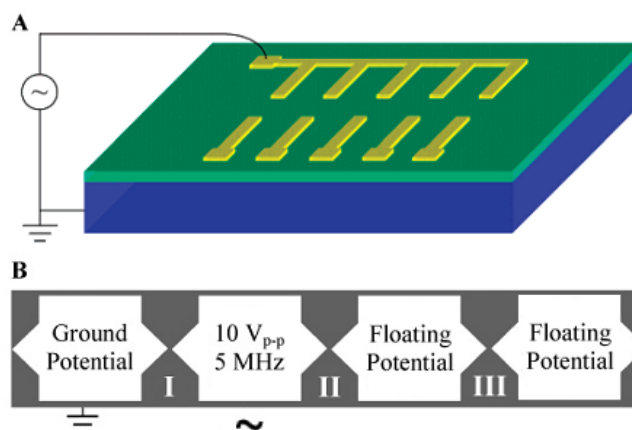
Figure 1.2 FPD geometries reported in the literature. A) This geometry biases a very large surface electrode against the underlying substrate; the CNTs are captured between a capacitively coupled row of electrically floating electrodes [30]. B) This geometry uses four surface-patterned electrodes; two are biased and two are floating [27]. The gap between the directly driven electrodes is used to catch nanotube aggregates and solution impurities, while the other two gaps are intended for primary use.

Several mechanisms have been proposed to explain the observed self-limiting behavior. For geometry A it was assumed that localized CNTs shorted the floating electrode to the driving electrode and thus eliminated the field necessary to localize more CNTs. For geometry B, a large number of CNTs and impurities were localized in region I, less in region II, and only one or a few CNTs in region III. It was assumed that since the voltage drop across the region I electrodes was greater than that of the region II electrodes, and the drop across region III less than either of the others, that the number of CNTs was simply proportional to the voltage drop in the region. Consequently, the self-limiting behavior of geometry B was assumed to be only a function of electrode potential.

A third mechanism was suggested in a report by Vijayaraghavan et al. due to measurements of geometry A indicating that CNTs did not short the electrodes. This mechanism was based on computational results showing that "once a CNT is localized between electrodes the local electric potential distribution (and thus the dielectrophoretic force-field) changes incisively and the region at and around the nanotube develops strong repulsive forces which prevent further CNT localiza-
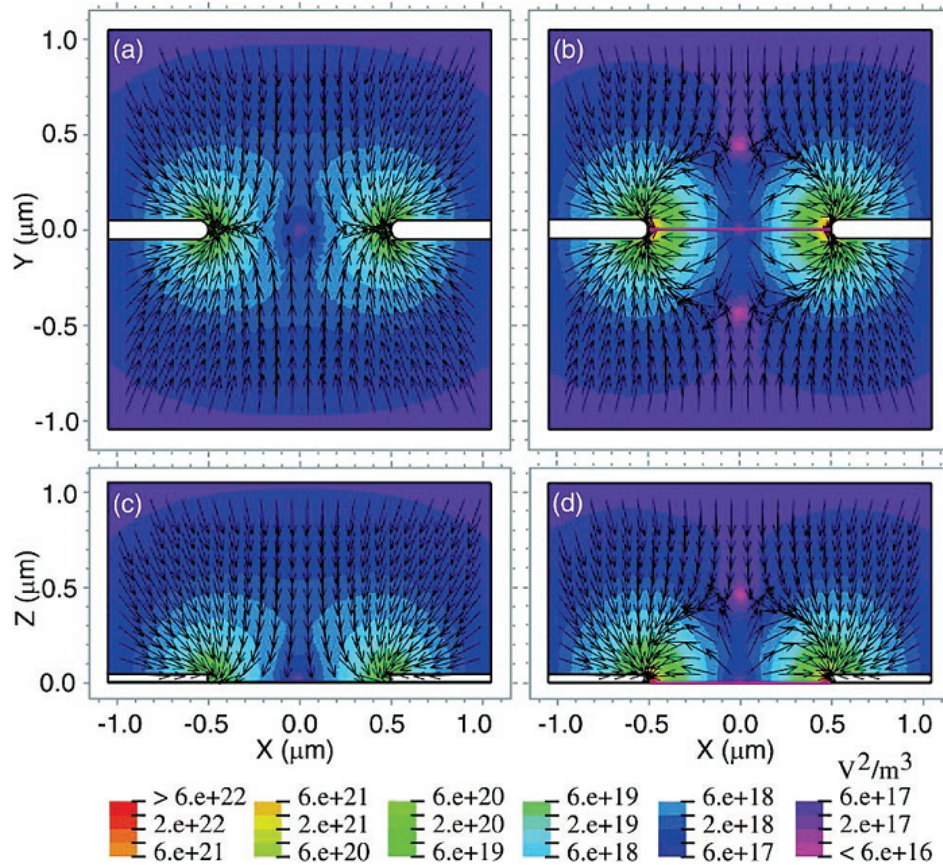
Figure 1.3 Most recent model for self-limiting FPD shutoff, from [24]. Top view: panes a) and b); side view: panes c) and d). Panes a) and c) are before localization occurs and b) and d) represent after a nanotube (purple) is localized. The arrows represent the direction of the DEP force and the color represents its magnitude. The boundary conditions on the electrodes were set to equal and opposite electric potentials, and since the resistance of the CNT is dominated by contact resistance, the CNT assumes a constant electric potential at the midpoint of the two electrodes.

tion" (see figure 1.3) [24]. This gradient-reversal model relies on the nanotube-electrode junction having a large contact resistance such that the voltage across the length of the tube is relatively constant compared to the drop at the electrode contact.

1.3 Motivation and Key Results

Interestingly, the boundary conditions used in the simulations introducing the gradient reversal model are compatible with directly driven DEP as well as FPD. However, it has been clearly observed that directly driven DEP does not always result in a limited number of localized CNTs (such as the inital studies of DEP using nanotubes, or even in region I of FPD geometry B). These apparent inconsistencies invite further investigation into the mechanism responsible for self-limiting localization of CNTs using DEP.

Furthermore, there are serious limitations imposed by the current FPD geometries. While a high device density has been achieved using geometry A, the necessity to couple each floating electrodes to the substrate imposes a $\sim 10 \ \mu\text{m}^2$ lower limit on floating electrode area [24] and restricts the technique to conductive substrates. While geometry B can be used on non-conducting substrates, it has not yet been demonstrated on a massive scale.

We report a geometry (figure 1.4) that allowed FPD to be performed using floating electrode areas more than an order of magnitude smaller than the limit of geometry A and which enables parallel FPD to be performed on non-conducting substrates on a massive scale. We also present computational results demonstrating that FPD using this geometry can be further scaled than what we experimentally demonstrated. By performing a series of experiments varying the duration of DEP, as well as experiments in which DEP was repeated on the same set of electrodes, we demonstrate that localized CNTs do prevent others from depositing, but only in their immediate vicinity. Our results clarify how the repulsive force behaves across length scales, and we discuss how scaling electrode width can be used to control the number of localized CNTs as devices continue to be scaled downward to smaller sizes.
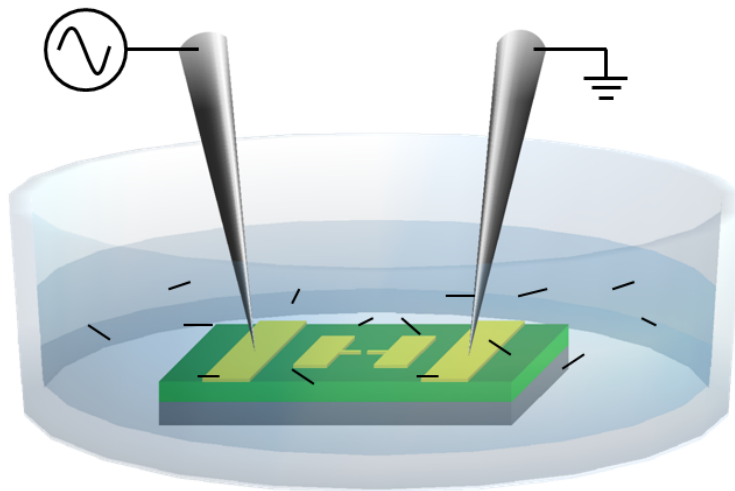
Figure 1.4 A cartoon image of the setup used in FPD experiments. The AC driving signal localizes nanotubes between the floating electrodes at the center of the image. Just like the cereal box, the CNTs are enlarged to show texture.

Chapter 2

Experimental Methods

2.1 Fabrication

The basic design of the FPD electrodes has an array of paired floating electrodes (FEs) in between two driving electrodes (DEs), as illustrated in figure 2.1. The DEs were 50-100 μm wide and scaled in length to match the length of the FE array. The FEs and DEs were separated by a gap of 1-10 μm. The FEs consisted of a 10-20 μm x 0.1-1 μm "finger" jutting away from a square pad which varied in area from 0 - 10^4 μm^2. Between each set of FE fingers was a 200-500 nm gap where the CNTs were intended to be localized, a region we refer to as the trap. Figure 2.2 is a flow diagram describing how the electrodes were fabricated.

2.2 CNT Purification

CNT suspensions were purified by isopycnic centrifugation (which separates CNTs by density, and thus chirality), following Arnold et al. [19]. Briefly, suspensions were prepared by sonicating 3-5 mg carbon nanotube soot (SouthWest NanoTechnologies SG76) in a solution of 2% (w/v) sodium cholate in water. The suspension was ultracentrifuged to remove large bundles of CNTs
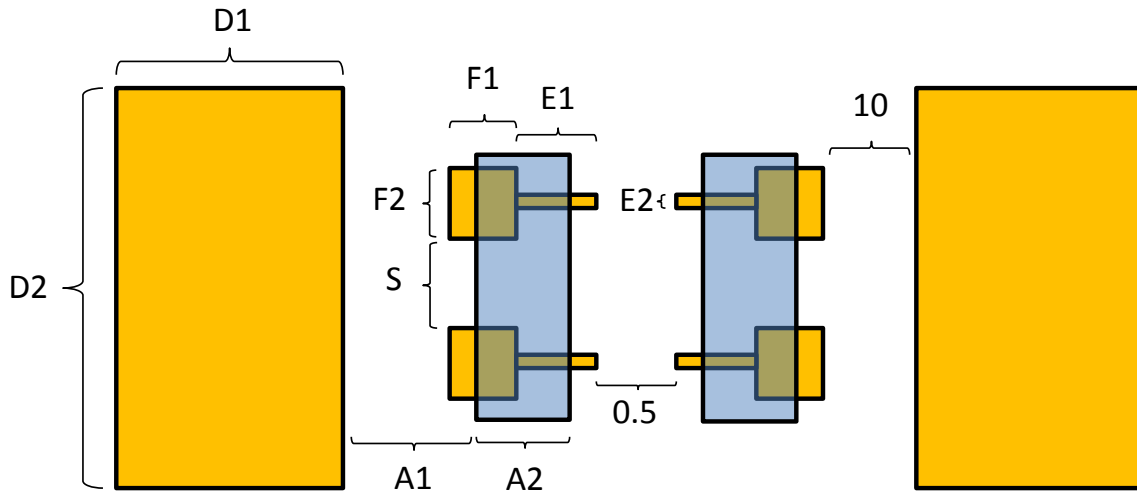
Geometry #	D1	D2	F1	F2	E1	E2	S	A1	A2
1	100	1820	100	100	20	1	20	0	0
2	100	1820	100	100	20	1	20	20	105
3	100	270	5	5	20	1	20	0	0
4	100	270	5	5	20	0.1	20	0	0
5	105	270	1	1	20	1	20	0	0
6	105	270	1	1	20	1	20	13	14
7	105	270	0	0	20	0.1	20	0	0
8	115	270	0	0	10	0.1	10	0	0
9	115	270	0	0	10	0.1	10	13	5

Figure 2.1 Cartoon layout of FPD geometries used in this work. Orange represents the electrodes and blue represents alumina. Units in the table are in microns.
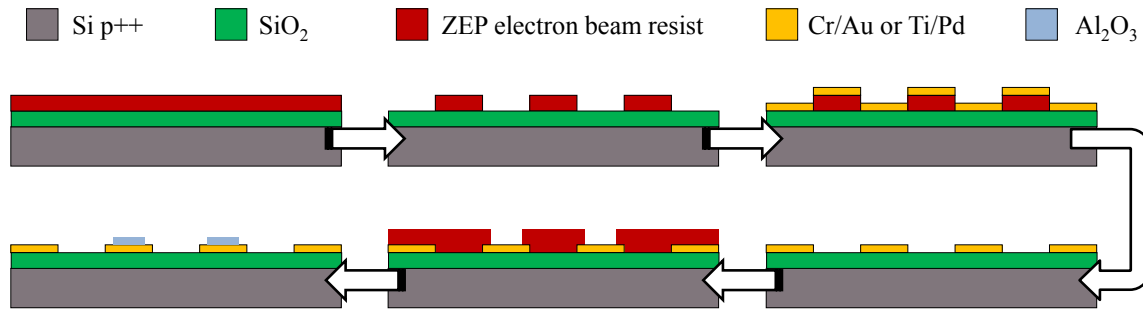
Si p++   SiO$_2$ ZEP electron beam resist   Cr/Au or Ti/Pd   Al$_2$O$_3$

Figure 2.2 A process flow diagram describing the fabrication of our FPD electrodes. In clockwise order: 1) ZEP 520A electron-beam resist was spun on a highly doped silicon wafer (Boron-doped, resistivity 0.002-0.005 Ω-cm) with up to 400 nm of SiO$_2$. 2) The resist was exposed and developed to create the electrode pattern. 3) Cr/Au or Ti/Pd was deposited on the substrate via electron-beam evaporation. 4) Microposit Remover 1165 was used for liftoff. 5) A new layer of resist was spun on the surface, and second pattern created with lithography aligned to the metal layer. 6) Aluminum oxide (alumina) was evaporated and liftoff performed as before.

and the growth catalyst. The supernatant was harvested and the tubes were concentrated by ultra-centrifugation. The concentrated tubes were put into a density gradient of 2% (w/v) sodium cholate (Sigma) in Optiprep Density Gradient Medium (Sigma) and ultracentrifuged again, resulting in the formation of distinct bands. The top two bands (which were pink and green, indicative of a high proportion of semiconducting CNTs) were harvested using a commercial fractionator (BioComp Gradient Station) and were used in this study.

We also dispersed CNTs in 1-cyclohexyl-2-pyrrolidone (CHP), a nonconducting solvent. This was done by sonicating 3-5 mg of the previously mentioned CNT soot in $\sim$10 mL CHP for 2 hr. The resulting dispersion was diluted in CHP or water for use in DEP experiments.

2.3 Dielectrophoresis

A signal of amplitude 1-20 V$_{pp}$ (Volts peak-to-peak) and frequency 50 kHz was generated using either an HP 3311A signal generator or an SRS 830 lock-in amplifier and electrically connected
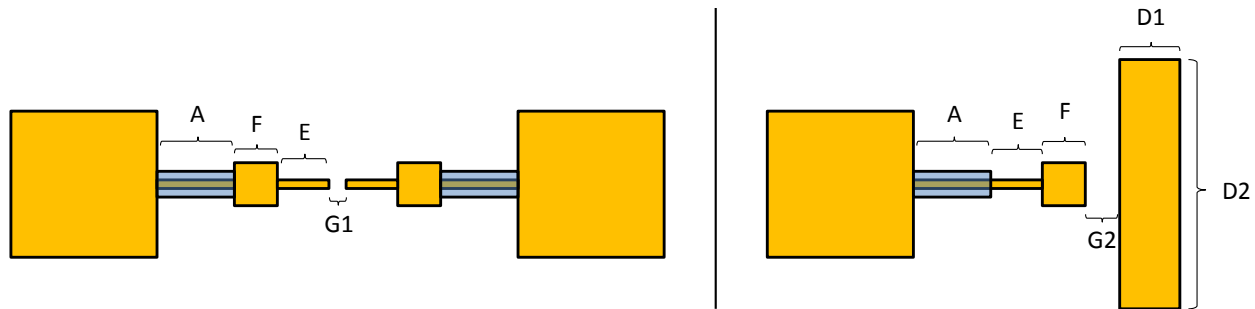
Figure 2.3 Geometries used for direct DEP experiments and for experiments to determine how the resistance between FEs (left) and between an FE and a DE (right) scaled as dimension F was varied between 0.5 - 100 μm. Dimensions G1, G2, E, D1, and D2 were 0.5, 10, 20, 100, and 1820 μm, respectively. The magnitude of A+E+F was held at 1 mm. The width of the long A and E electrodes was 1 μm. The configuration on the left, with F = 100 μm, was used for direct DEP experiments.

to the DEs with micromanipulators. Two methods were used to perform DEP. In the first, the die containing the electrodes was covered in deionized water and a 2 μL drop of the previously described suspension added directly above the trap. In the second method, the CNT suspension was diluted in water and a ~30 μL drop was added to the dry FPD microelectrodes. In both methods, the micromanipulator probes were removed after 60 s and rinsed in deionized water (for water-based suspensions) or N-methyl-pyrrolidone (NMP) and isopropanol (IPA) (for CHP-based suspensions). For water-based CNT solutions, deionized water was added to the dish containing the sample to flush the CNT solution out, and the sample was then rinsed briefly in a stream of deionized water and dried. For CHP-based solutions, the sample was taken from the dish and was rinsed in IPA.

DEP was also performed by directly driving electrodes of size and shape similar to the FEs used in our FPD experiments. To avoid displacing a large volume of solution by inserting a probe immediately above the electrodes, we fabricated insulated leads connecting the electrodes to bonding pads as shown in figure 2.3.

For both FPD and direct DEP, captured CNTs were imaged with a Dimension V AFM (Bruker)
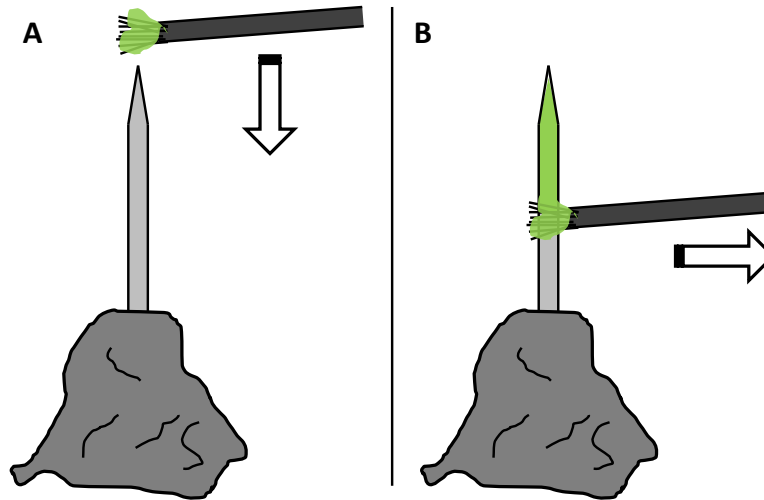
Figure 2.4 A) Needles were pressed into a stand made of aluminum foil and the nail polish brush lowered directly through the needle apex. B) The brush was removed horizontally. The sharpness of the needle apex caused the polish to wick away, leaving a very small region of the apex uncoated.

in tapping mode. Height, phase, and amplitude data were taken.

2.4 Electrical Measurements

2.4.1 Probe Modification

Micromanipulator probes used in electrical measurements were modified by coating them in an electrically insulating fingernail varnish (Orly International) as described in figure 2.4. The varnish was allowed to dry for several hours and the coating procedure repeated until the exposed apex measured less than 50 μm via SEM (see figure 2.5). If the apex was over-coated with a thin layer, probes were inserted into the micromanipulator and rubbed against the sample surfaces until they became electrically conductive. If the apex was over-coated in a thick layer it was cleaned in acetone and dried, and the coating procedure was repeated.

Top View

Side View

Acc.V	Spot	Magn	Det	WD	Exp		10 μm
5.00 kV	3.0	5000x	SE	12.6	1		

500 μm
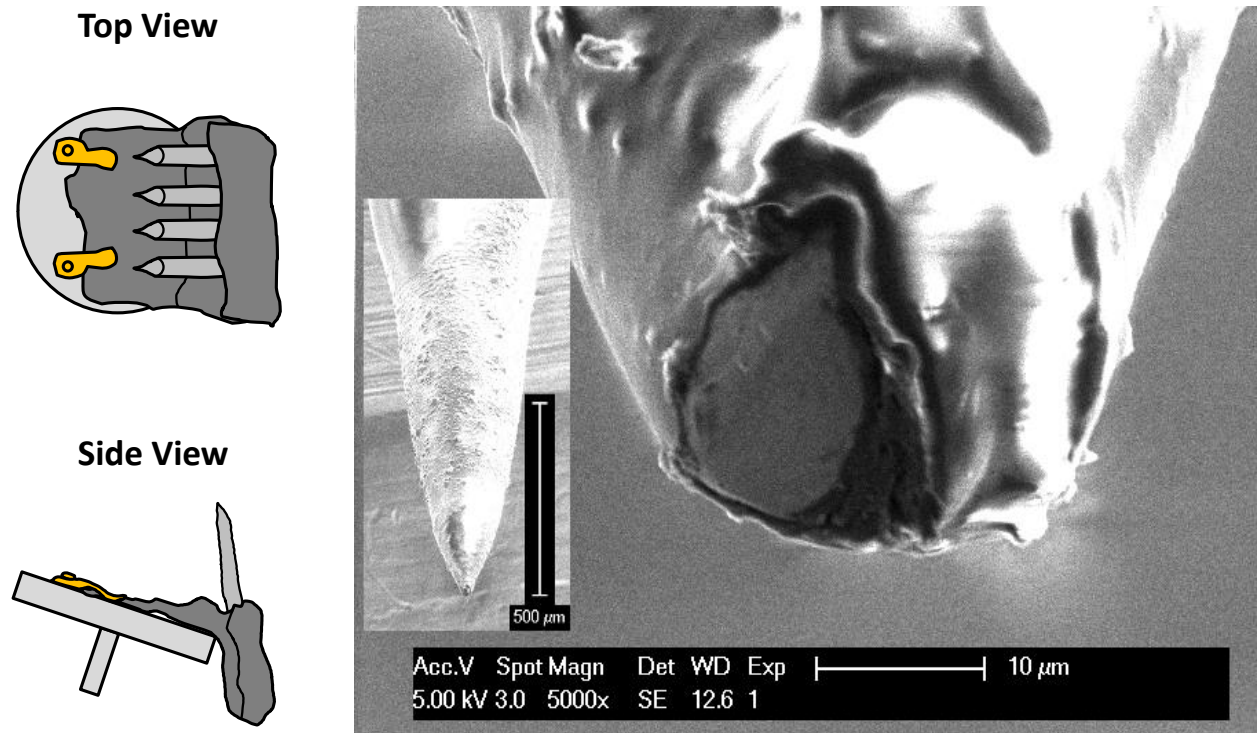
Figure 2.5 Left: Cartoon image showing how the needles were mounted to position and stabilize them for SEM imaging. The aluminum foil basket both served as a carrying case as well as conductive medium to ground the needles during imaging for high contrast. In this way the exposed conductive region of the needle could be easily seen through the insulating nail varnish. Right: SEM micrograph of a micromanipulator probe insulated at all but the apex.

2.4.2 Impedance Measurements

Impedance measurements were taking using an HP4192A impedance analyzer and programs written in LabVIEW, which are included in Appendix A.1.

To measure the impedance between the various electrodes for use with our lumped element analysis model (which is discussed in Section 4.3.1), a variation of geometry 1 described in Section 2.1 was fabricated (see figure 2.6). A polydimethylsiloxane (PDMS) and insulated leads connecting the FEs to large bonding pads were employed for to: 1) avoid directly inserting the probes above the FEs (which would displace a large volume of solution), and 2) avoid coupling the probes on the FEs to the solution itself (as then the measurement would be dominated by the resistance between the probes through the solution rather than measuring the impedance from electrode to electrode).

To determine how the resistance between electrodes scaled with FE size, impedance measurements were taken using the electrode geometries in figure 2.3. This geometry was specifically needed for measurements involving FE sizes smaller than $\sim 30\ \mu$m, because the probe was larger than the FE and could not be contacted accurately.

To measure fluid conductivity, 2-point measurements were taken using an HP4192A impedance analyzer with a driving signal of 1 V$_{rms}$ at a frequency of 50 kHz. The analyzer was connected to a pair of 1 mm diameter nickel wires inserted into opposite ends of a 1.1 mm diameter heparinized glass capillary tube (Chase Scientific Glass) as shown in figure 2.7. The wires were pushed in the tube until $\sim$1 mm apart, and the tube was suspended slightly in the air by hanging the connecting wires such that there was a slight downward tilt. A micropipette was touched to the top of the tube and $\sim$30 μL of the fluid to be measured was slowly inserted until the fluid flowed past the junction between the two wires. The wires were pulled apart in 1 mm intervals and the impedance measured at each distance. The conductivity was then extracted by modeling the measurement as a cylindrical volume of fluid contacted at both end by the metallic contacts.
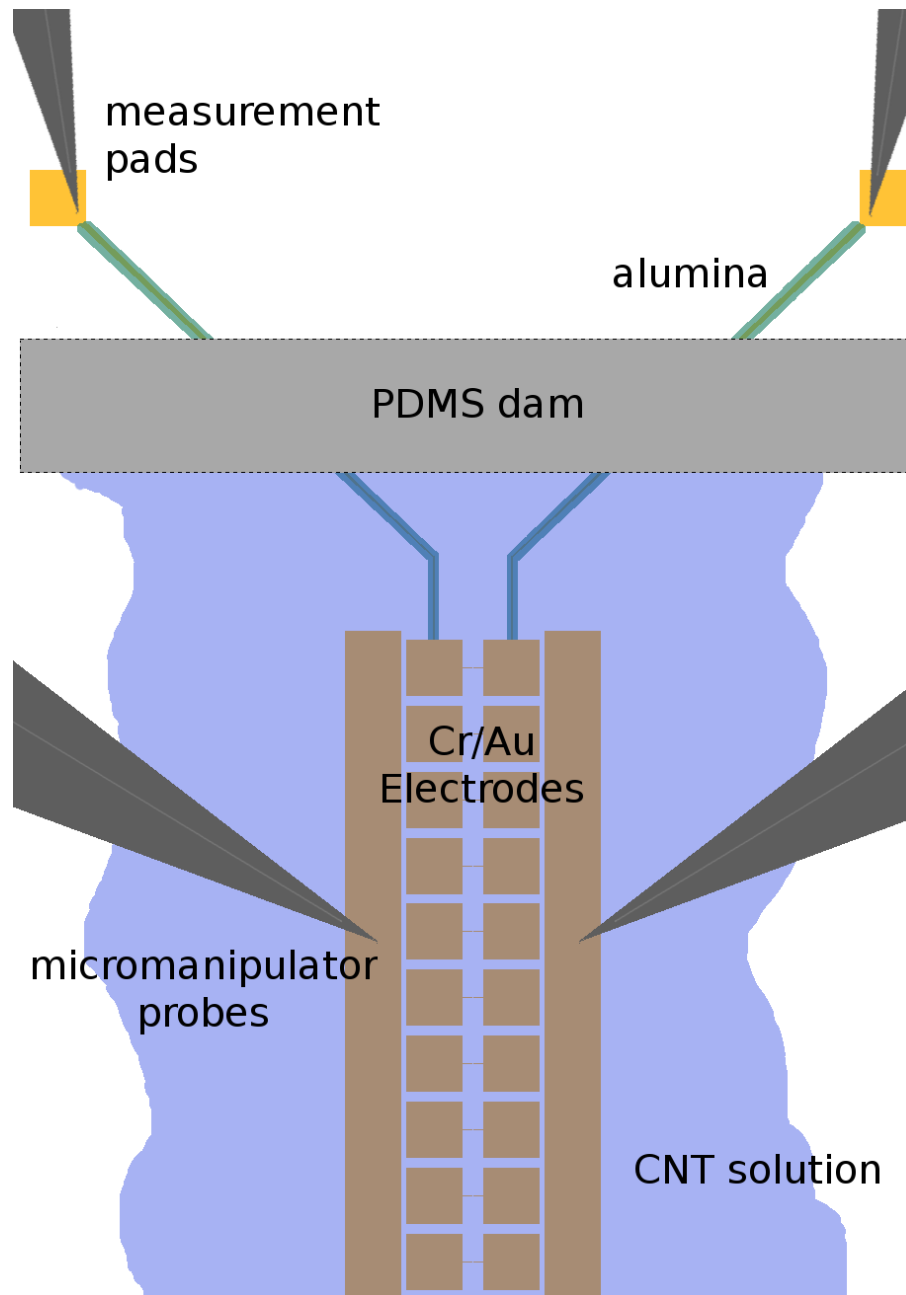
Figure 2.6 Cartoon image of the PDMS dam configuration used in impedance and voltage measurements. Leads were drawn from the top two FEs of the array to bonding pads located approximately 1 mm away from the device and covered in alumina to insulate them from the surrounding solution. A 5 mm x 0.1 mm x 1 mm dam was carved out of a sheet of PDMS using a razor blade and inserted over the leads to keep the probes from contacting the solution. A series of 2-point measurements were made between various electrodes to determine the lumped parameters (for example, the resistance between a DE and an FE was measured by connecting the impedance analyzer to the probe on one of the DEs and the probe behind the dam connected to the closest FE).
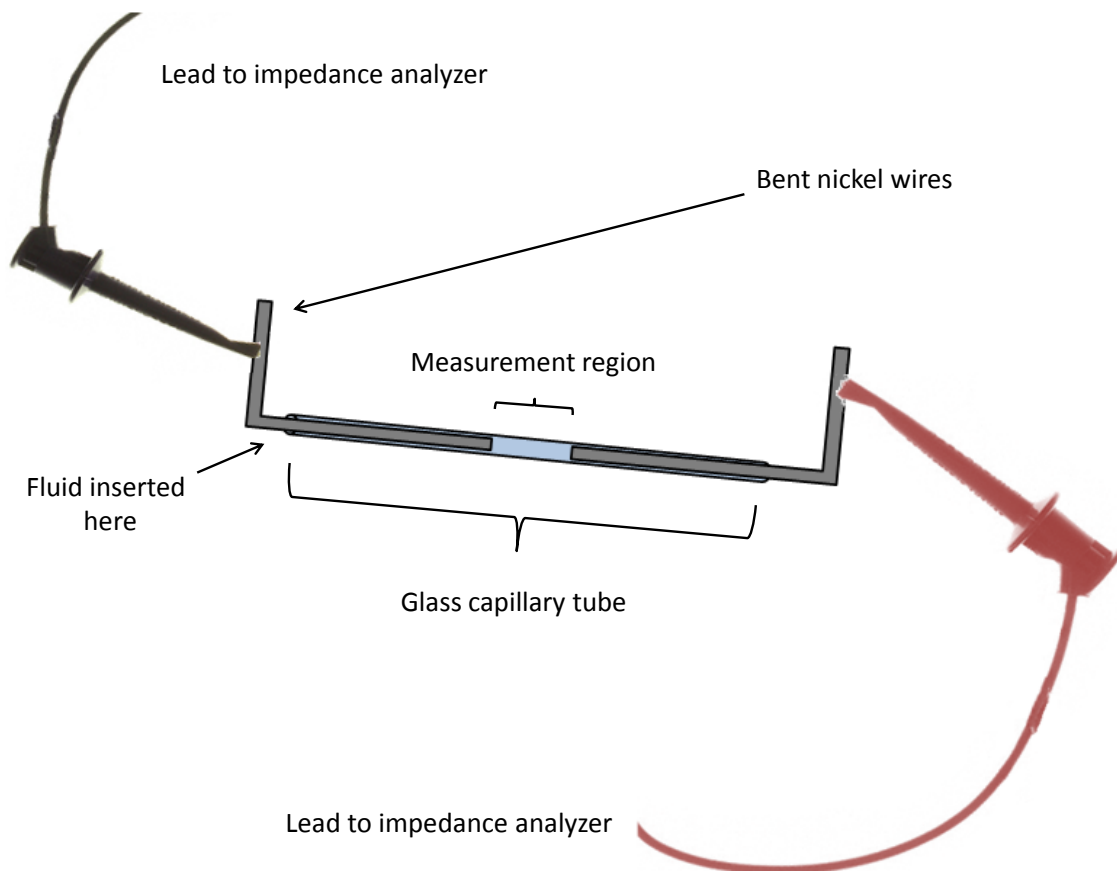
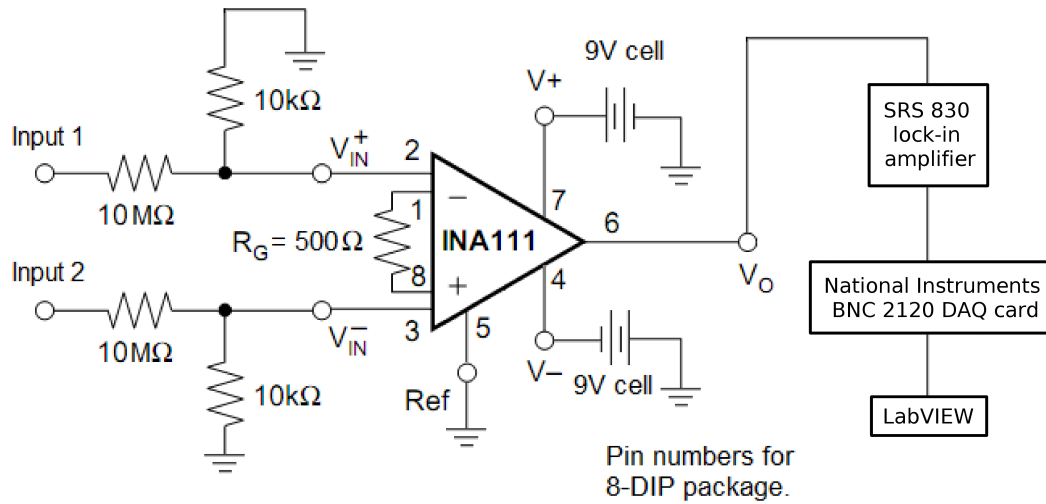**Figure 2.7** Cartoon image of apparatus to measure fluid conductivity.

Figure 2.8 Schematic for high input impedance AC potentiometer.

2.4.3 Voltage Measurements

I custom-built a potentiometer to accurately measure the AC voltage drop between electrodes without loading the FPD circuit. To realize this, an IC instrumentation amplifier with a large common-mode rejection ratio (INA111AP-ND, Burr-Brown) was utilized for accurate measurements. To yield low parasitic input capacitance even at high frequencies, a voltage divider constructed from hand-matched carbon-composition resistors was used as a buffer, and the circuit was mounted inside of a rigid nonmetallic box. A schematic is shown as figure 2.8. After construction, the measured input capacitance was less than 0.3 pF. Measurements were performed on electrodes with insulated leads and a PDMS dam as described in Section 2.4.2. The LabVIEW program used to read data from the meter is included in Appendix A.1.

Chapter 3

Results

3.1 Geometry and Voltage Dependence

We initially expored our new FPD geometry by varing the voltage applied to the DEs to determine how the number of CNTs localized in each trap changed as a function of applied voltage. Figure 3.1 shows that a minimum voltage of $\sim$8 V_{pp} applied to the DEs was necessary to localize CNTs in FPD experiments. We also performed experiments in which the FEs were directly driven (as discussed in section) to compare with experiments from the literature. Figure 3.2 shows that slightly larger than 3 V_{pp} was necessary for CNTs to be localized in these experiments. In both cases, beyond this threshold voltage, the average number of localized CNTs increased with applied voltage, though it can be seen that the slope of this increase was dependent on which method was used to insert the CNT solution. When the CNT solution was added to the dish of water (see Section 2.3), the slope was highly dependent on the size of the FEs, but FE size had little or no effect on the slope when the "premixed solution" was dropped onto dry electrodes.

Varying the size of the "fingers" between FEs (see figure 2.1) also changed the number of localized CNTs. Figure 3.3 shows traps of geometry 8, where the FE finger linewidth was 0.1 μm

19
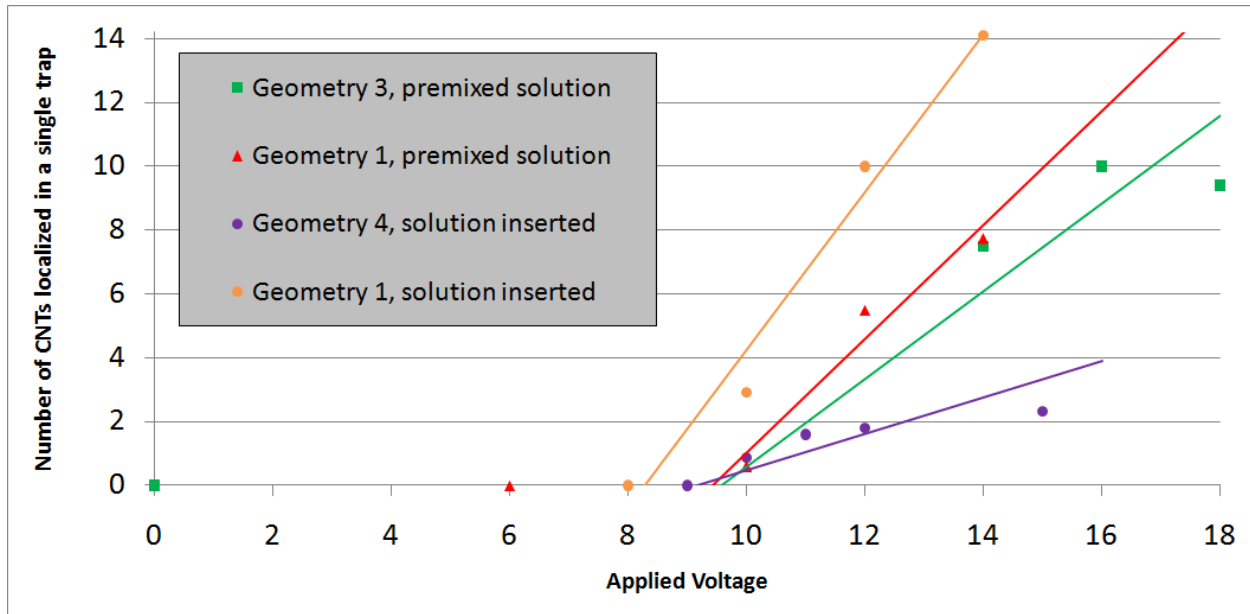
Figure 3.1 Comparison of the two methods of FPD used in this study: when the CNT suspension was added to the die in a dish of water, and when the suspension was diluted in water and added to dry electrodes. Each data point represents an average of ~ 10 devices. Error bars have been ommitted for clarity.
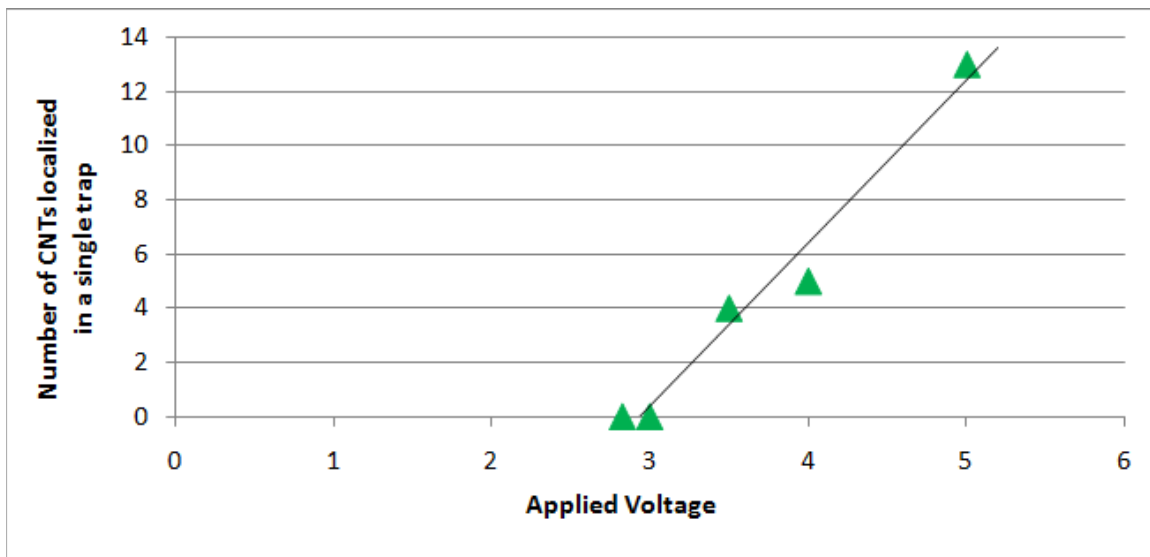
Figure 3.2 Results of experiments applying a voltage directly to 100 μm square FEs, using the geometry of figure 2.3. This behavior is very similar to the results of FPD on these FEs (see figure 3.1), but the voltage threshold was much lower and the slope nearly three times steeper.
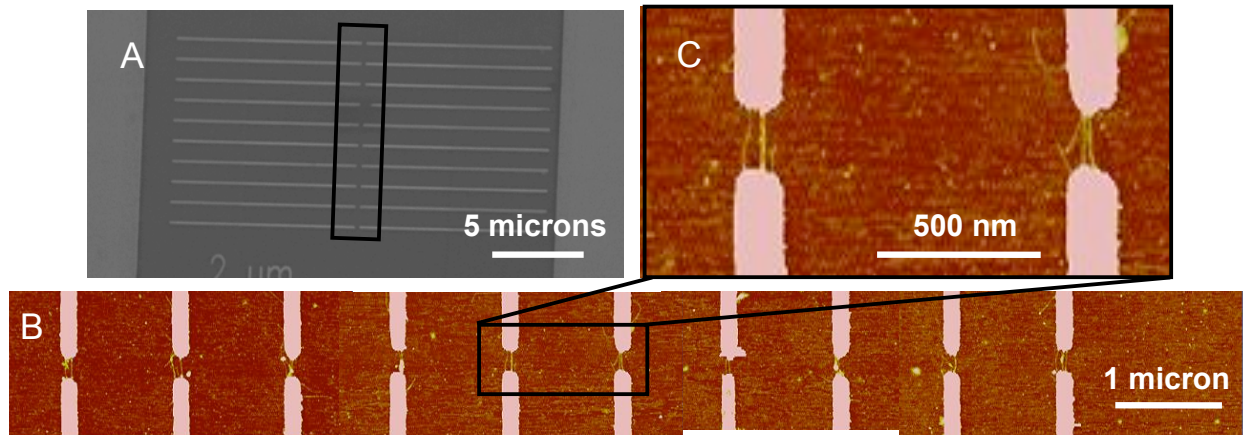
Figure 3.3 SEM (A) and AFM height images (B-C) of geometry 8 devices. These devices captured only 2-3 CNTs between each pair of electrodes, in contrast to the larger devices shown in figure 3.4.
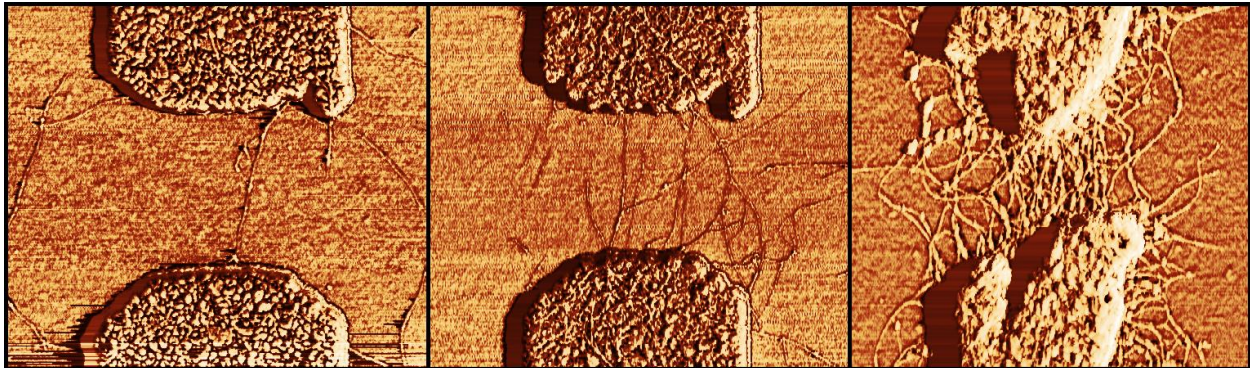
Figure 3.4 AFM phase images of geometry 5 devices with 1 μm wide FE fingers. While the devices with smaller FE fingers shown in figure 3.3 captured at most 4 CNTs, these larger devices often captured many more CNTs. Depending on the voltage and FE size, anywhere from 0 to 33 CNTs were observed captured in these larger devices. Images are 2 μm wide on a side. Irregularities in electrode shape were due to writing glitches during electron-beam lithography exposure.

wide. In over 100 devices of this size, there were never more than $\sim$ 4 CNTs bridging the gap.

In contrast, figure 3.4 shows several traps of geometry 5, where the FE finger linewidth was 1 μm

wide. The larger devices captured up to 33 CNTs.

3.2 Time Dependence

After performing DEP and imaging to count CNTs, DEP was performed again on the same devices to determine whether more CNTs could be localized. On over twenty geometry 1 devices, traps with large numbers of tubes captured few, if any, more (figure 3.5 A-B), while traps with few tubes captured many more (figure 3.5 C-F).

To then determine whether CNT localization was a function of the duration of the driving signal, we performed DEP for varying amounts of time rather than the usual 60 s. For geometry 1 devices, the number of localized CNTs increased with time, but the rate at which CNTs were captured diminished with time (see figure 3.6 A, E).

To investigate whether the rate diminished due to a local absence in concentration, diffusion effects were calculated as follows. At room temperature, for CNTs of length $L = 1\mu$m and diameter $d = 1$ nm, and fluid viscosity $\eta = 1$ mPa-s, the diffusion coefficient [31] is:

$$D = \frac{k_B T \ln(L/d)}{4\pi\eta L} \approx 2.3 \ \mu\text{m}^2/\text{s}. \tag{3.1}$$

Using this diffusion constant, the characteristic length over which CNTs can diffuse during the 60 s time scales of our experiments is therefore $2\sqrt{Dt} \approx 23.5\mu$m. From optical absorbance data, we can estimate that our nanotube density is on the order of $10^9/\mu$L, or $1/\mu\text{m}^3$. At this density, a hemispherical region of radius equal to the diffusion length contains greater than three orders of magnitude more CNTs than were ever trapped in our devices. We conclude from this calculation that the decrease in the CNT localization rate is not diffusion limited.

3.3 Impedance Results

Figure 3.7 is a plot of impedance data taken on geometry 1 devices before and after dielectrophoresis, both with and without CNT solution. Contrary to the report of Vijayaraghavan et al., which
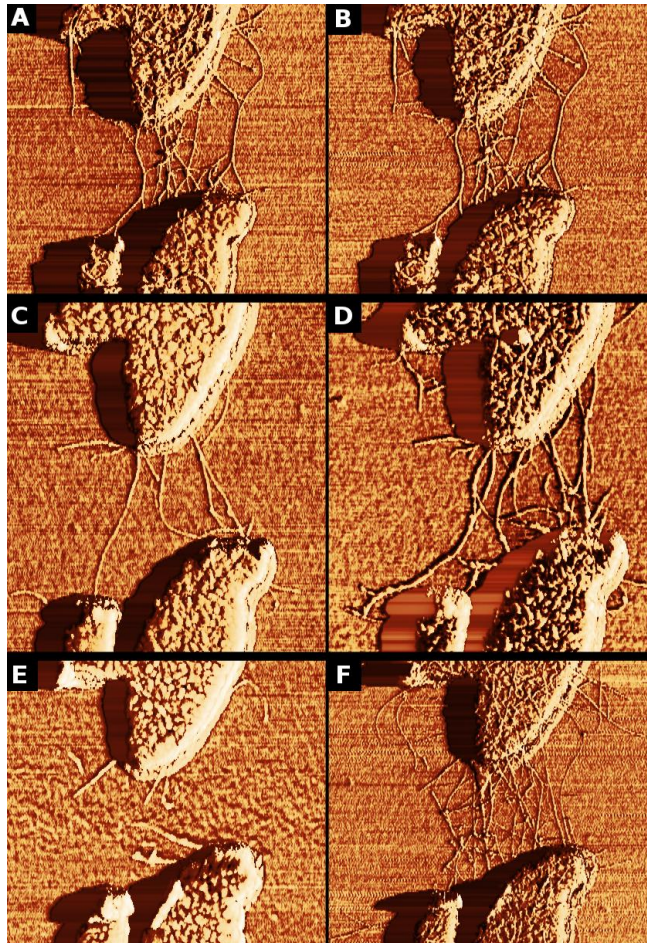
Figure 3.5 AFM height data; images are $\sim 2\ \mu$m on a side. A,C,E: After the first iteration of FPD. B,D,F: After performing FPD on A,C, and E, again, respectively. These images are representative of experiments performed on over twenty electrodes. Irregularities in electrode shape were due to writing glitches during electron-beam lithography exposure. For these experiments, where the purpose was to determine whether CNTs could be localized on devices after DEP had already been performed once, this did not appear to compromise results.

showed an insignificant change in trap impedance before and after dielectrophoresis, our measurements showed a significant decrease ($\sim$30%) in impedance upon CNT localization. In making these measurements, we observed that standard probe station probes compromised measurement results in fluid. Specifically, it was essential to modify the probes with insulating material every-
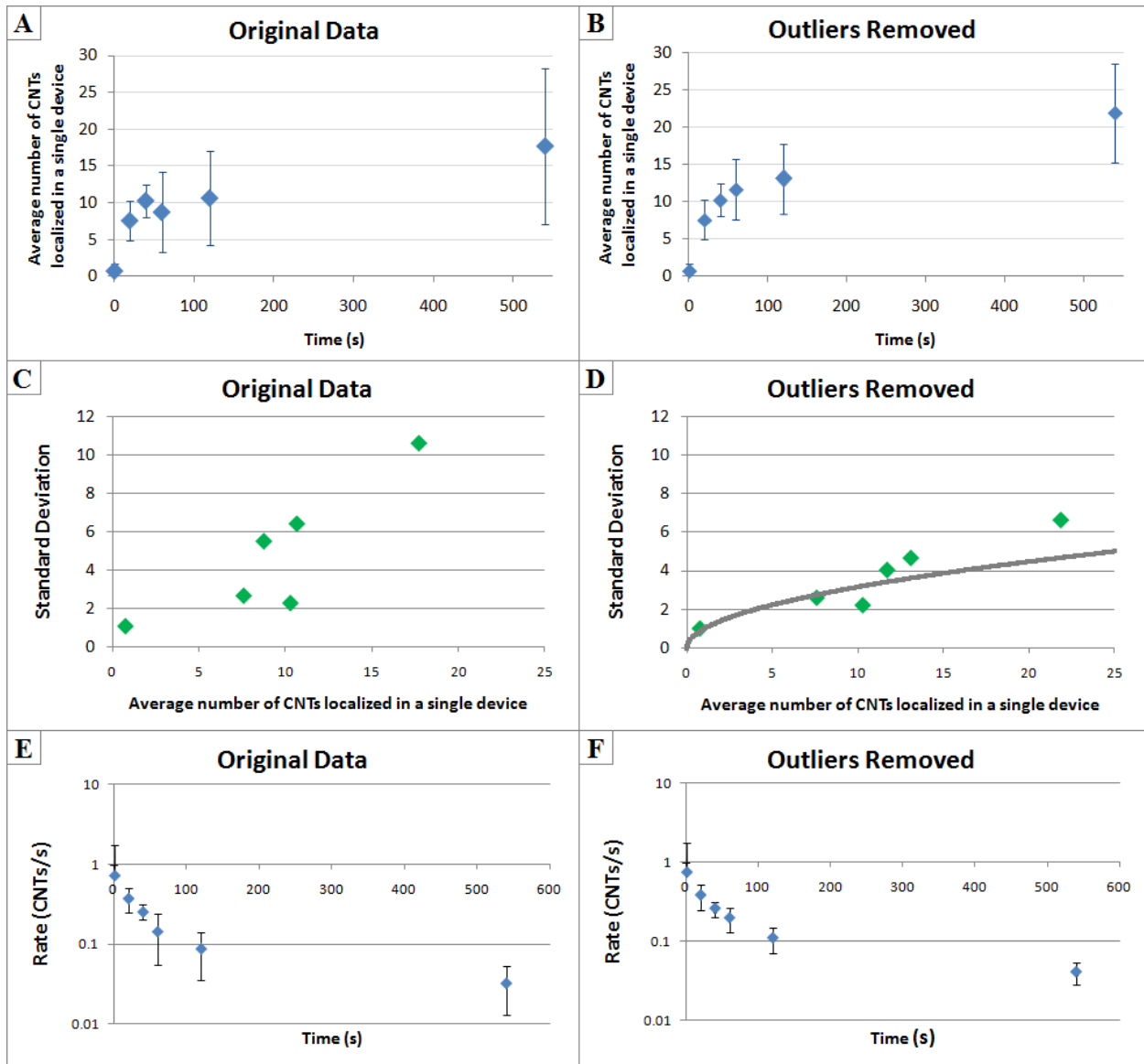
Figure 3.6 Results of experiments in which the duration of DEP was varied on geometry 1 devices. The rates in E-F were obtained by dividing the average number of captured tubes by the duration of DEP. As discussed in Section 4.1, the outliers referred to are those devices which erratically captured far fewer tubes than average. While there is significant variation in all FPD experiments, it is clear from comparing the two sets of data in this figure that removing these outliers produces reliable counting statistics. From the agreement shown in figure 3.6 D of standard deviation to the square root of CNT number, we infer that CNTs are randomly distributed from trap to trap as they are pulled from solution.

Figure 3.7 Impedance across the trap region of geometry 1 devices, as measured with probes electrically insulated everywhere but the apex. Red: in the absence of CNT suspension, the FEs are only capactively coupled. Green: after CNT suspension was put on the surface, but before DEP was performed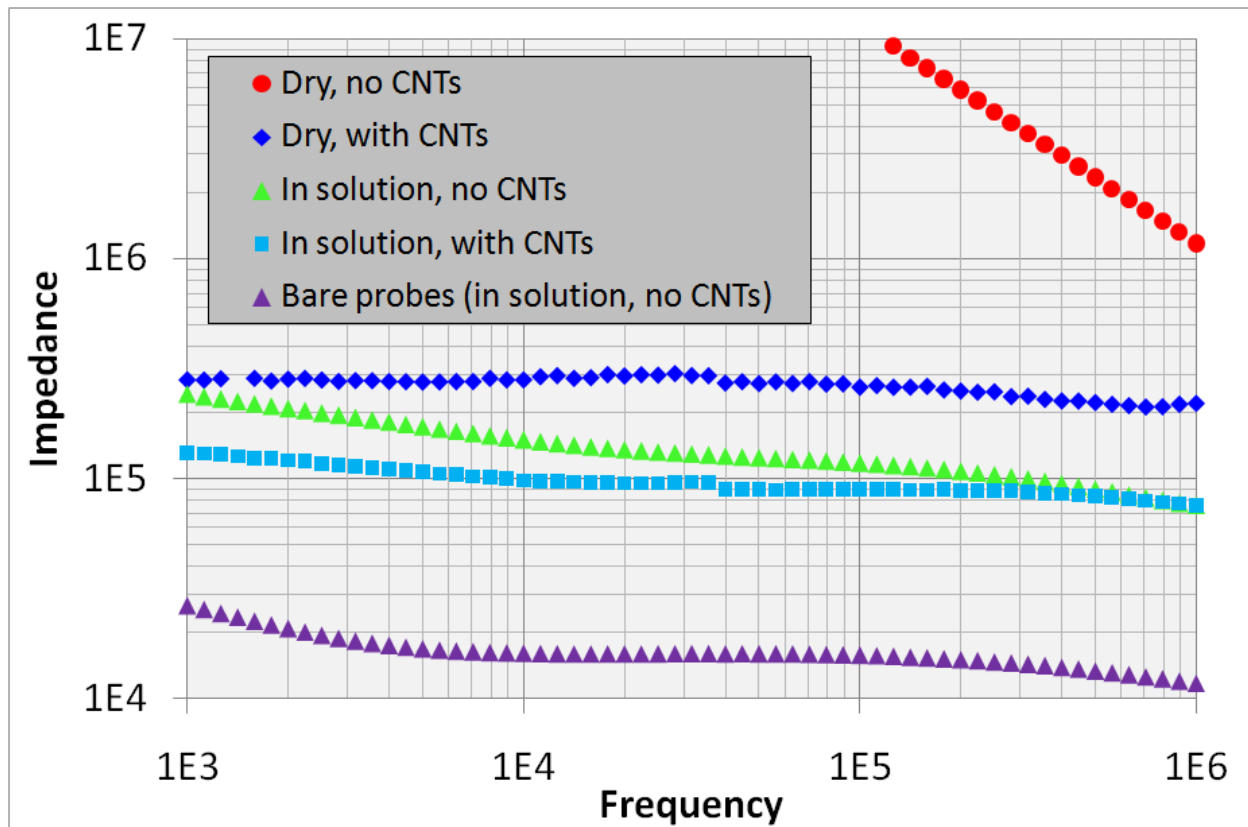, resistive coupling dominates the impedance between the FEs. Cyan: CNT localization caused trap impedance to drop (approximately 30% at 50 kHz). Blue: when the trap was dried, the blue curve shows a purely resistive CNT impedance of approximately 300 kΩ. Purple: a measurement in surfactant solution with standard (e.g., not coated) probes is also shown for reference. While the particular trap this measurement was performed on was not imaged, other traps that were run under the same conditions captured ∼4 tubes.

where but at the apex. Coated probes gave trap impedances of ∼125 kΩ at 50 kHz, whereas bare probes produced only ∼16 kΩ.

Figure 3.8 is a measurement of the impedance between electrodes as FE size was scaled downward. The geometries sketched in figure 2.3 were used in these measurements. As FE area de-
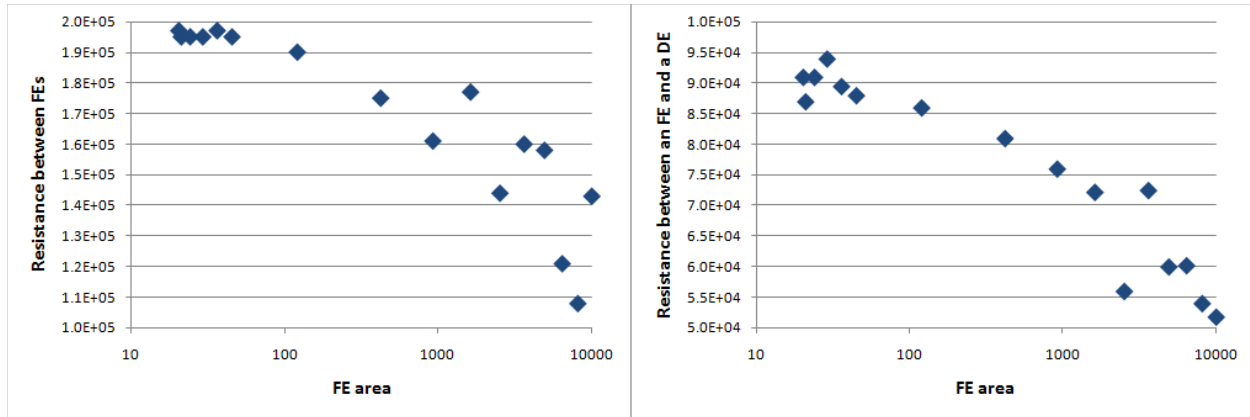
Figure 3.8 Measured resistance between an FE and a DE (left) and between FEs (right) as a function of FE area. The geometry of figure 2.3 was used for these measurements. This data indicates that as FE area decreases, the resistance between the various electrodes increases.

creases, the resistance increases as would be expected from a spreading resistance model. For a given CNT resistance, this implies that localizing a CNT would cause a greater change in impedance upon localization for smaller FEs.

3.4 Spatial distribution of CNT localization

AFM data showed that CNTs were localized primarily in the trap region between the FEs, including tubes that both partially and completely bridged the gap. CNTs also were also observed on the FE surface with a density that decreased with distance away from the gap. Localized CNTs were observed in the DE to FE gap when the gap was 4 μm or smaller, and occasionally near sharp areas such as narrow electrodes or corners of bonding pads.

Depositing aluminum oxide (alumina) was sufficient to prevent CNTs from attaching in un-wanted areas. For example, when we deposited an alumina strip over the gap between the DEs and the FEs, CNTs were prevented from making electrical connection and "shorting" the FEs to the DEs. When alumina was deposited to partially cover the FEs for the experiments described in
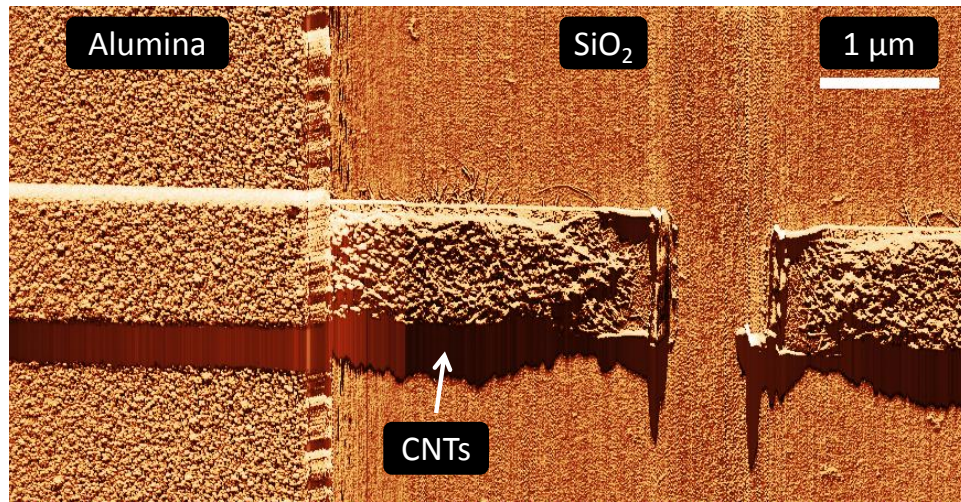
Figure 3.9 Composite AFM amplitude image of region near the trap. A large portion of the region is covered in alumina (left). Bare areas of the FEs (which run left and right through the center of the image) can be seen in the immediate vicinity of the trap. A large mat of CNTs has been localized on all of the other parts of the FEs not covered in alumina.

Section 4.3.2, CNTs were only localized on the exposed portion of the FE, as shown in figure 3.9.

Chapter 4

Discussion

4.1 Elucidating the Shutoff Mechanism

I will now discuss our experimental results and their implications for furthering parallel dielectrophoretic localization of CNTs. At first glance, the raw data in figure 3.6 A shows standard deviations nearly as large as the average number of CNTs. However, the results of the experiments presented in figure 3.5 indicate that some devices capture far fewer tubes than expected from the average (for example, the device in figure 3.5 E). Figure 4.1 shows a histogram of the number of captured tubes in devices where DEP was performed for 540 s. While there is a fairly even distribution centered around the average of 22 CNTs, there are two devices which erratically captured very few tubes. These devices may be the result of large contamination particles localized to the trap or bubbles formed in the trap due to hydrolysis; such phenomenon would prevent CNT deposition during DEP, but would be removed during the rinse step.

In addition to the fact that these devices lie far outside the normal distribution of tubes, removing these outliers from the data can further justified by examining the number of captured CNTs vs standard deviation. When the outliers are removed from this data, the standard deviation goes very
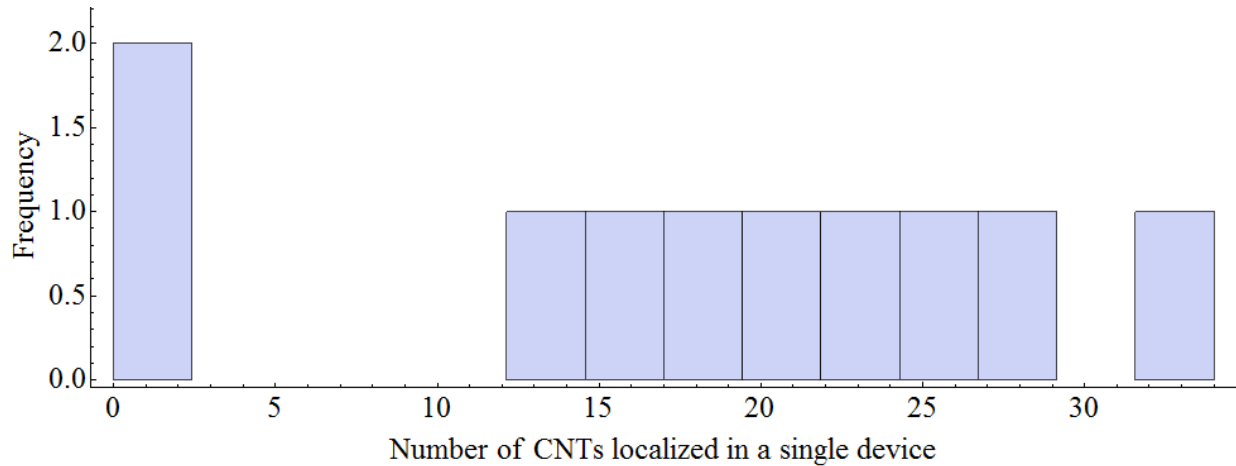
Figure 4.1 Histogram of data showing the number of CNTs localized in each trap when DEP was performed for 540 s, the average of which forms one of the data points in figure 3.6 A. The data is distributed fairly evenly around the average of 22 localized CNTs, except for the two devices which captured an unusually low number of CNTs at the left.

closely as the square root of tube number (compare figure 3.5 C and D). This relationship would be expected if CNTs were randomly distributed from trap to trap. From this examination we can infer that removing devices with unusually low numbers of CNTs produces reliable data, even for these small sample sizes. For reference, figure 3.6 B and F show the average tube number vs. time and the rate vs. time replotted with these outliers removed.

The results presented in Section 3.2 indicate that if given enough time, CNTs will continue to deposit until the trap region is generally covered with a rough layer of tubes. This behavior is consistent with the self-limiting mechanism postulated by Vijayaraghavan in 2007 [24]. However, contrary to their assertions, our data indicates that junctions which capture multiple tubes are not always the result of simultaneous deposition. Furthermore, the data indicates that the DEP shutoff mechanism is not always binary, meaning that a device is not completely "on" or completely "off" after the first CNT is localized. Rather, the repulsive force generated upon CNT localization is only local in its effects, and CNTs can continue to deposit preferentially on areas not immediately occupied by other CNTs. Figure 4.2 is a finite element analysis simulation illustrating that in
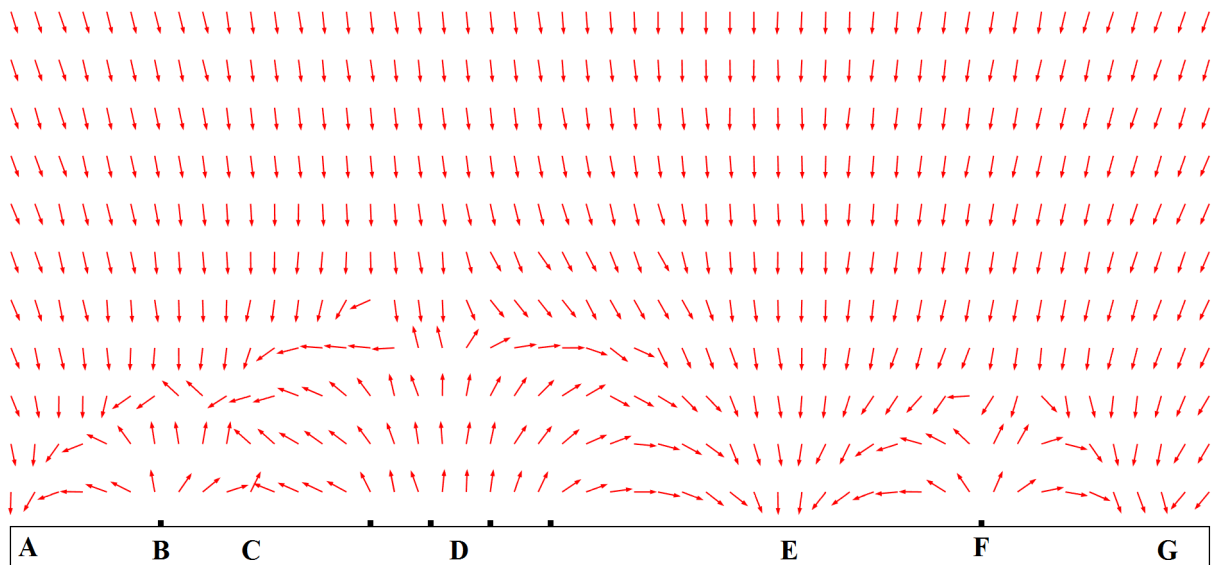
Figure 4.2 Finite element analysis simulation results representing the direction (not magnitude) of the DEP force when CNTs are partially covering a wide aspect ratio electrode. In this y-z slice cut taken at the midpoint of the trap, six CNTs (represented by the small black squares at points B, D, and F) point into the plane of the page and sit on top of a 1 μm wide electrode (whose extent is represented by the white rectangle) at the bottom of the image. Arrows pointing up and down represent a repulsive and attractive force, respectively. Immediately above points B, D, and F the nanotubes cause a repulsive force, with the extent of the repulsion at D larger than at B and F because there are four CNTs at D. At points A, E, and G the force is attractive toward the bare region of the electrode. Though there is a bare region at point C, the CNTs at B and D are close enough that the force is repulsive, illustrating that more CNTs can continue to deposit preferentially on areas not immediately occupied by other CNTs.

regions of high CNT density the DEP force is repulsive but in regions of lower CNT density an attractive force is still present.

The local nature of the repulsive force suggests that trap width is the determining factor for the maximum number of CNTs that can be localized at each junction. Comparing the results in figures 3.3 and 3.4 shows that far fewer CNTs were localized in the 0.1 μm wide devices than in the 1 μm wide devices. In fact, the wider geometry 6 devices captured an average of 7.7 $\pm$ 2.9 CNTs, while the narrower geometry 9 devices captured 2.8 $\pm$1.3 CNTs. These observations are consistent with

the observations of Vijayaraghavan et al. in which no more than ~4 CNTs were localized on their 0.1 μm wide electrodes.

This fact that narrow trap electrodes capture few tubes can also be seen from the data taken on geometry 4 devices in figure 3.1. The data shows that these devices, which have 0.1 μm "fingers" at the trap region, captured very few CNts even for very large applied voltages. Furthermore, while the other data in the figure show a linearly increasing trend, it appears that the trend for the geometry 4 devices begins to "cap out" at large applied voltages. This may be an indication that if narrow devices are only capable of capturing few tubes, this maximum is asymptotically being reached as voltage increases.

4.2   Scaling to Smaller Sizes

In the geometry we present in this work, the coupling between the DEs and the FEs is dominated by fluid conductivity (figure 3.7), which circumvents the requirement of previous geometries to have FE area large enough to achieve capacitive coupling to the substrate. This allowed us to fabricate FEs smaller than the minimum limit previously achieved in the literature (as discussed in section 1.3). Additionally, our lower limit was only due to lithographic limitations, and we fully expect that single- or few-CNT devices can continue to be obtained as this geometry is scaled downward. In fact, fininte element analysis simulations using our geometries showed that as electrode dimensions were reduced, the magnitude of the DEP force increased, implying that less voltage may be sufficient to achieve the same results.

While most of the geometries employed for CNT-counting purposes consisted of ~15 traps per set of DEs and covered less than 1 mm^2, we have also fabricated a geometry that was used to capture CNTs on a greater-than 1 cm^2 scale. These devices consisted of sets of 5 x 1 μm FEs arranged between interdigitated 10 μm wide DEs, separated by a 2.5 μm gap with 3 μm spacing
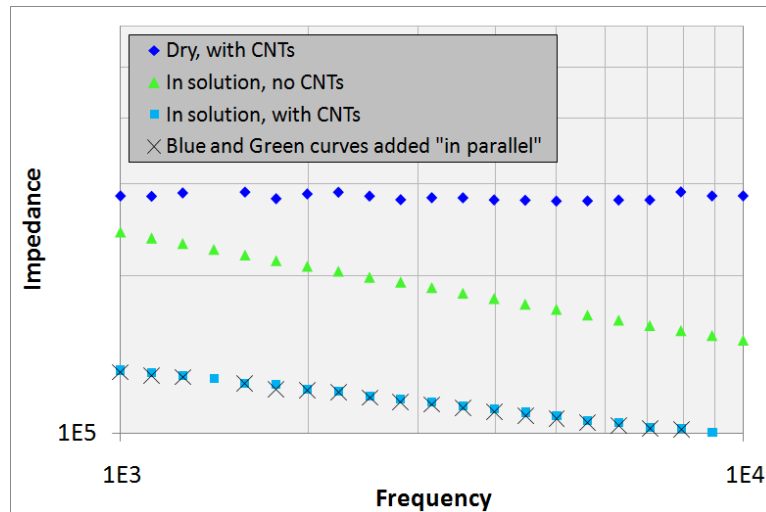
Figure 4.3 A zoomed in portion of the data presented in figure 3.7. The X's mark calculated data points of adding the dry measurement of CNTs in parallel with the measurement of electrodes in solution without CNTs. The agreement of this calculation with the measured data indicates that these measurements are valid and that the CNTs can cause large changes in impedance bewteen the FEs as they are localized.

between FEs. This corresponds to a device density of $\sim$1 million devices per cm^2, illustrating that not only can this geometry be used to scale individual CNT devices smaller, but can maintain high device density over large surface areas.

4.3   The Search for an Additional Shutoff Mechanism

Figure 4.3 highlights a portion of the impedance spectroscopy data from figure 3.7. From a conceptual standpoint, adding the measured impedance of the electrodes with solution added but without localized CNTs "in parallel" with the measured impedance of the dry localized CNTs should be equivalent to the measurement of the electrodes in solution with CNTs. Figure 4.3 shows this calculated data overlaid on the measurement. The agreement is quite accurate, indicating that the measurements are a valid representation of the system we are measuring.

While not enough experimental details were provided to reproduce the impedance spectroscopy measurements of Vijayaraghavan et al., which implied that CNT localization produces an insignificant change in impedance, our measurements with coated probes in figure 3.7 show that CNT impedance is quite significant in our system. This is likely due to our use of coated probes, which decrease the contact area between the probe and the fluid by several orders of magnitude.

This discussion indicates that in addition to the gradient reversal observed and discussed earlier, an additional shutoff mechanism may be possible: if localized CNTs significantly change the impedance, it is possible that in certain regimes localized CNTs could cause a reduction in voltage on the FEs large enough to "turn off" the DEP force. This is especially relevant considering the results of figure 3.1, which shows that a reduction in voltage will lower the number of captured CNTs and, in fact, could entirely shut off the device if the voltage drops below the threshold required for localization. Thus, while our measurements show that it is not likely that the large contact resistance between the localized CNTs and the electrodes would entirely short the FEs, a binary shutoff may still be possible if a CNT localization causes a change in potential enough to dip below the threshold. This would essentially be a way to enable the superb results of the limiting resistor experiments discussed in Section 1.2 to be used on a massively parallel scale.

This prospective mechanism is even more interesting considering our measurements of the resistance between electrodes as a function of FE area, presented as figure 3.8. As earlier noted in figure 3.7, the localization of $\sim$300 kΩ of CNTs caused a $\sim$30% change in impedance for large FE area. Figure 3.8 shows that as the FEs are scaled to smaller sizes, the resistance between the electrodes increases, implying that nanotube localization will cause a greater change in impedance and have a greater chance to reduce FE voltage below the threshold, causing binary shutoff.
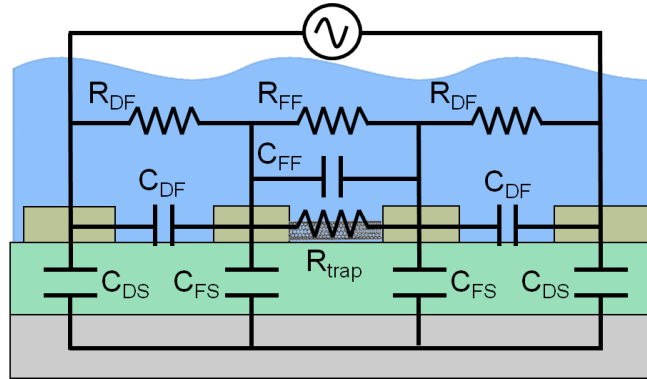
Figure 4.4 Circuit representation of an FPD device. To model CNT localization we noted that the dielectrophoretic force is proportional to the voltage across the FEs, which we calculated using lumped element analysis. The gaps and fluid between electrodes were treated as capacitors and resistors, respectively. Subscripts abbreviate electrodes: D is driving, F is floating, and S is substrate; for example, C_{FS} is the capacitance between an FE and the substrate. R_{trap} denotes the variable resistance of the carbon nanotube(s) captured in the trap.

4.3.1   Lumped Element Analysis Modeling

We modeled the system impedances using lumped element analysis as shown in figure 4.4. The dielectrophoretic force is proportional to the gradient of the electric field intensity as shown in equation 4.1 [17].

$$F = \frac{\alpha}{2}\nabla|E|^2 \tag{4.1}$$

The term α in this equation is the polarizability of a carbon nanotube in an electric field.

The driving electric field can be approximated as a dipolar field that is proportional to the voltage difference across the FEs (i.e., across the trap). By approximating the trap as a dipole of length d with charge +Q on one FE and -Q on the other, the capacitance between the FEs is expressed as C_{FF}=Q/V_{trap}, where V_{trap} is the voltage difference across the FEs. The dipole moment is then expressed as $\vec{p} = Q\vec{d} = (C_{FF}V_{trap})\vec{d}$. The gradient of the electric field intensity for

this dipole can then be calculated (see Appendix A.2), and equation 1 becomes:

$$F = \frac{\alpha C_{FF}^2 V_{trap}^2}{16\pi^2 \varepsilon_0^2} \nabla \left| \frac{3\hat{r}(\vec{d} \cdot \hat{r}) - \vec{d}}{|\vec{r}|^3} \right|^2 \tag{4.2}$$

Here r is the distance between the center of the trap and the carbon nanotube, and $\hat{r}$ is the unit vector of r.

This short range force is proportional to $|V_{trap}|^2$, which we calculated using lumped element analysis. The gaps and fluid between the various metal electrodes were treated as capacitors and resistors, respectively, and the carbon nanotube was treated as a variable resistor. A schematic of this simple circuit is shown in figure 4.4B. The voltage difference across the FEs was calculated in terms of these parameters (see Appendix A.2):

$$|V_{trap}|^2 = \frac{\beta \, V_{app}^2}{(2/R_{trap} + \zeta)^2 + \xi^2} \tag{4.3}$$

where $V_{app} \sin \omega t$ is the voltage applied to the DEs, the reactance terms $X_i = 1/(\omega C_i)$, and

$$\beta = \frac{1}{R_{DF}^2} + \frac{1}{X_{DF}^2}, \quad \zeta = \frac{1}{R_{DF}} + \frac{2}{R_{FF}}, \text{ and } \xi = \frac{1}{X_{DF}} + \frac{2}{X_{FF}} + \frac{1}{X_{FS}} \tag{4.4}$$

are geometrical constants. The other variables are identified in figure 4.4B.

We have compared this model with several aspects of our experimental results. Figure 3.1 indicates that no CNTs were captured below $V_{app} = \sim 8 \, V_{pp}$. Equation 4.3 implies that if there is a threshold in V_{app} then there is also a threshold in V_{trap}. Using resistance and capacitance values directly measured on the modified geometry 1 devices of figure 2.6, we calculate $V_{trap,threshold} = 3.5 \pm 0.17 \, V_{pp}$. We tested this threshold by applying a driving voltage directly to the FEs, and observed a threshold onset at slightly larger than $3 \, V_{pp}$ (see figure 3.2). This is in good agreement with the calculation.

Our observation of a voltage threshold (figures 3.1-3.2) is similar to a recent report of a minimum electric field necessary to localize CNTs [32]. However, dividing the voltage threshold of
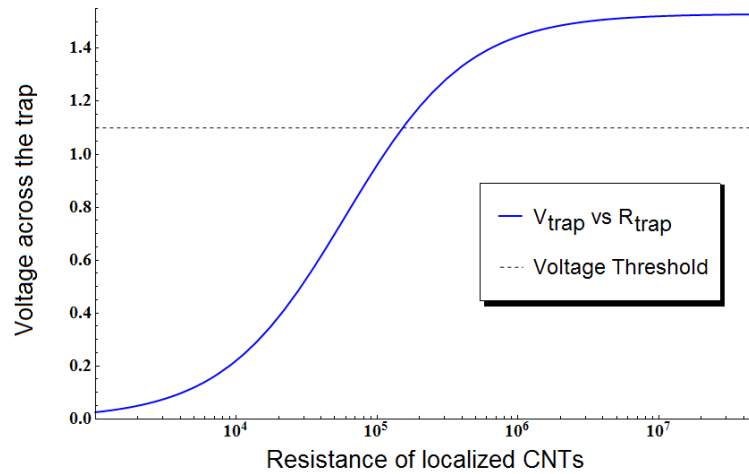
Figure 4.5 Plot of equation 4.3 with respect to R_{trap} capacitance and resistance values measured using the geometry of figure 2.6. As a device localizes CNTs R_{trap} decreases. Once R_{trap} is sufficiently low $|V_{trap}|^2$ (proportional to the dielectrophoretic force) is small and the device no longer attracts tubes.

$\sim$3 V$_{pp}$ for directly driven FEs by the gap size of the trap ($\sim$500 nm) to calculate an electric field strength gives a magnitude approximately 6 times larger than reported value in the literature.

Equation 4.3 shows how V_{trap} changes as CNTs are captured in FPD, which we plot as a function of R_{trap} in figure 4.5. Before we start dielectrophoresis, R_{trap} is infinite. As CNTs are localized, R_{trap} decreases, consequently reducing $|V_{trap}|^2$. When V_{trap} drops below the threshold, no more tubes are captured.

Using resistance and reactance values measured on geometry 1 devices, equation 4.3 predicts an expected change in voltage of $\sim$20% upon CNT localization. However, monitoring trap voltage during DEP produced no observable change in voltage during DEP (figure 4.6). As the data of figure 3.6 suggests that CNTs are continuously localized for several minutes after DEP begins, it is not possible that all CNT localization took place as the solution was added. Despite the $\sim$30% change in impedance, the expected voltage change was not observed.
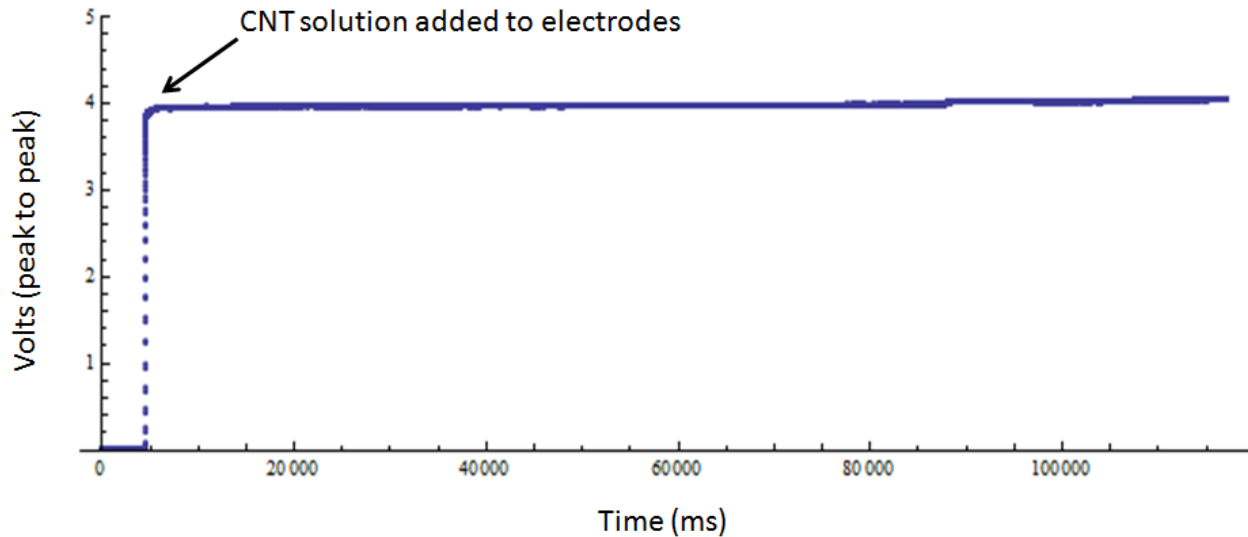
Figure 4.6 Plot of measured voltage on the FEs during DEP. The voltage on the DEs was 14 V_{pp}. Despite millisecond temporal resolution no voltage changes larger than a few mV were detected, though the lumped element analysis model predicted changes on the order of 500 mV.

4.3.2 Finite Element Analysis Modeling

While the lumped element analysis model predicted some things very well, we did not observe one of its key predictions. We conducted finite element analysis simulations using Comsol Multiphysics (included in Appendix A.2). From initial simulations it became clear that we were missing a significant piece in our lumped element analysis: the fluid potential above the electrodes was dominated by a gradient between the micromanipulator probes used to drive the system, as shown in figure 4.7. Because the fluid potential varies continuously across the region between the driving electrodes, lumped element analysis may have been conceptually valuable but was not well-suited to quantitative analysis of this problem.

The fact that there is a gradient between driving electrodes also explains why we did not observe a voltage change on the FEs upon CNT localization. The potential on the FEs indeed is affected in part by the coupling due to CNT localization, but it is also governed by the large sur-
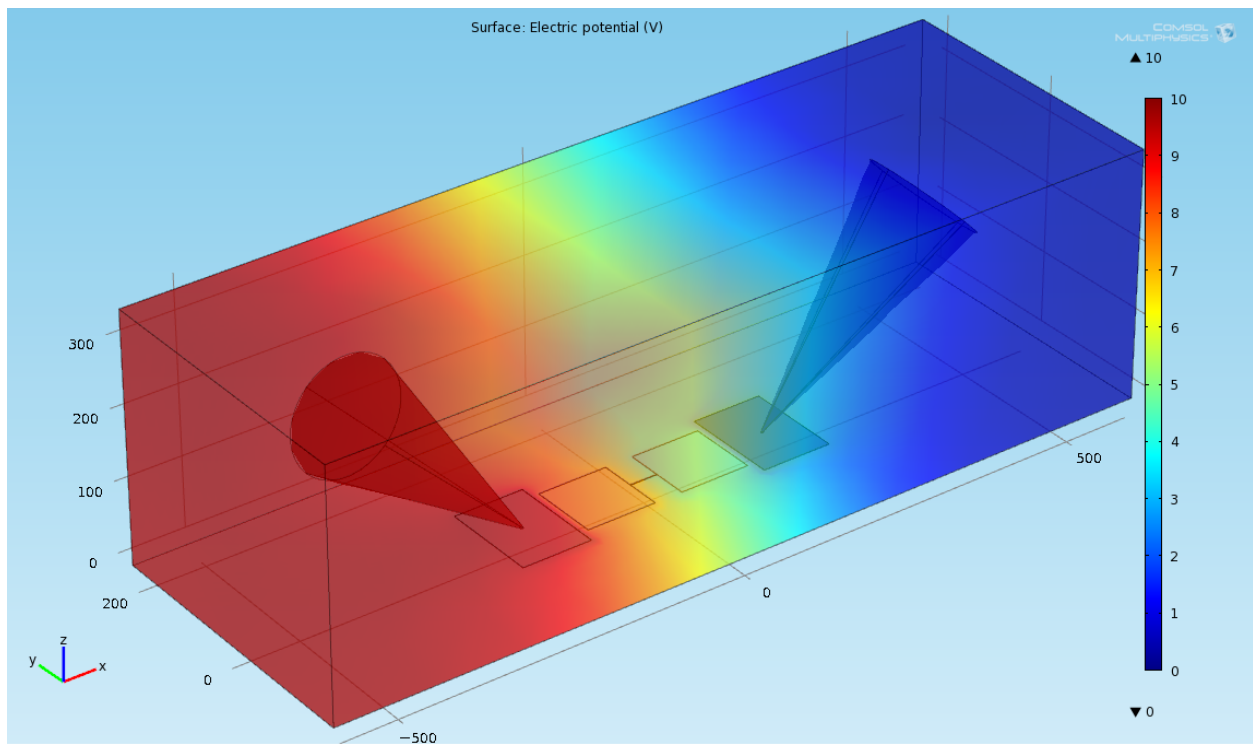
Figure 4.7 Finite Element Analysis simulation of the potential surrounding the geometry 1 system. It is clear to see the gradient in fluid potential between the driving electrodes and that the potential on the FEs is held by a sort of "weighted average" of the fluid potential immediately above them.

face area of metal in contact with the fluid. When no CNTs are present in the simulation, the voltage on the FEs was essentially a "weighted average" of the fluid potential immediately above them. Unless the CNT resistance was remarkably low, FE potential was essentially fixed by the high conductivity of the fluid.

These simulations sparked a new direction in our search for an additional shutoff mechanism. As earlier noted, a group of CNTs with impedance 300 kΩ caused a ∼30% change in impedance for geometry 1 devices (figure 3.7. Our simulations showed that if the fluid conductivity were lowered, 300 kΩ of CNT resistance would cause a very large reduction in V_{trap}. Alternatively, if the geometry were altered such that coupling of the FEs to the fluid was greatly diminished, the coupling to each other through the CNTs would become much more important.

From earlier data taken in our group, only 2 CNTs (of 23 measured) had resistance larger than 1 GΩ. We therefore investigated geometries in which changes in V_{trap} were larger than 40% even for contact resistances up to 100 MΩ, with a larger change for CNTs with less contact resistance. Because a ∼20% change in V_{trap} would be more than sufficient to cause shutoff to occur, in these regimes no more than a few CNTs should ever be localized before statistics would indicate that one well connected CNT would shut the device off.

These geometries were created by depositing alumina across the middle of the FEs, leaving small regions of the FE uncovered near the DE-FE gap and the trap (see geometries 2, 6, and 9 of figure 2.1). It was noted that for FE areas less than ∼10 μm^2, alumina was not necessary for voltage changes upon CNT localization, though it did increase the magnitude of the change and improved the drop for CNTs with high contact resistances. Despite the results of our modeling, however, figure 4.8 A is one device representative of many that captured very many CNTs, indicating that the expected shutoff mechanism was not present.

Another approach we investigated was adding the insulating solvent CHP to our solutions, as described in Section 2.2. Simulations showed three regimes as solution conductivity dropped: the
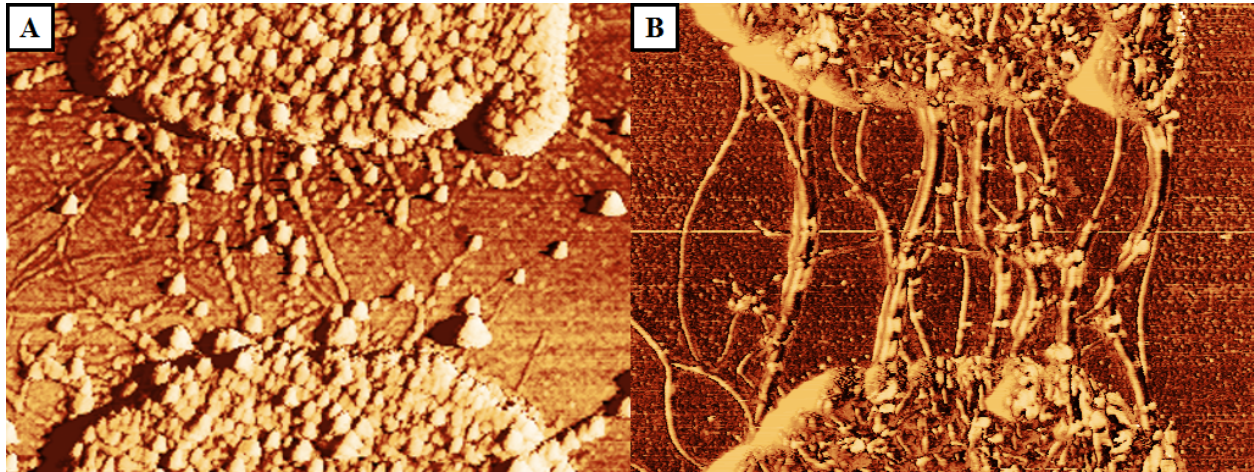
Figure 4.8 AFM phase data showing many localized CNTs. A) Using geometry 6 to decouple the FE from the fluid in an attempt to more closely couple the FEs together after CNT deposition. B) Using highly resistive fluid to have a more dramatic effect upon CNT deposition. These results were typical of many devices, indicating that binary shutoff was not operative under the tested conditions.

first was that in highly conductive solution the FE voltage did not change at all, as previously discussed; the second is that there would be a large voltage change as we were expecting to find; and as the conductivity dropped low enough the electrodes were no longer resistively coupled and the FE voltage was no longer above the voltage threshold in the absence of localized CNTs. A series of dilutions was used to make the solution less conductive, including CNTs dispersed directly in CHP, which had a measured conductivity less than 5 μS/m. Though this conductivity was so low that the experiments should have been in the third regime, figure 4.8 B shows that many CNTs were localized. The voltage drop across the FEs must have been above the threshold voltage, but apparently there was not a change in voltage large enough to cause shutoff behavior, even in incredibly resistive solution.

While these results don't detract from our conclusion that electrode width is the determining factor for the number of CNTs that are localized, the discrepancy between the experiments and our computational results is too striking to ignore. Either a significant factor has been neglected in our

modeling, or else something else is responsible for the behavior we have observed. For example, there could be mobile ions in solution that raise the conductivity very near the surface, or perhaps plasmon effects from the gold surfaces could be interfering with DEP. These results invite further investigation in the study of dielectrophoresis.

Chapter 5

Conclusion

I have here presented results demonstrating that the number of localized CNTs has a nonlinear dependence on applied voltage, the length of time DEP is performed, and trap electrode width. These results, made possible using a geometry that allows further scaling of massively parallel FPD, elucidate the local and non-binary nature of the self-limiting mechanism governing the maximum number of localized CNTs. With recent discoveries about carbon nanotube purifications [20], this work enables the fabrication of densely packed few- or many-CNT devices of only one electronic type, on both non-conducting or conducting substrates.

We have investigated an alternative shutoff mechanism based on our data regarding impedance changes upon CNT localization. Our modeling indicated that significant impedance changes would cause shifts in trap voltage low enough that devices would no longer attract CNTs. Finite element analysis modeling showed that in the geometries we explored, these changes would be greater for lower solution conductivity. While much has gone into this investigation of an alternative shutoff mechanism, our results are definitive: the number of CNTs is no more limited in non- or weakly conductive solution than in highly conductive solution. It is apparent that an effect not included in our modeling is operative and perhaps dominant, which prevented the voltage on the FEs from changing dramatically as CNTs were localized.

43

Appendix A

LabVIEW Progams and Modeling Code

I will here include brief descriptions and images of the labVIEW software and modeling code used for this research. Digital copies can be found at http://dl.dropbox.com/u/4938827/Modeling.html.

A.1   LabVIEW Programs

- Fastsweep is based on the National Instruments provided instrument drivers that controls the HP4192A impedance analyzer. It allows you to measure impedance while either frequency or voltage is swept, with a variety of options. The data is then saved to a spreadsheet.

- Realtime Impedance is software that reads output from the HP4192A impedance analyzer as a function of time and records the data to a spreadsheet. The program formats the raw data in an intelligible format according to the type of information read from the instrument.

- Realtime Voltage is software that reads output from the potentiometer (detailed in Section 2.4.3) via a NI-DAQ card.

Because impedance sweeps are limited by instrument's measuring capabilities at low frequencies, Fastsweep was only mildly optimized optimized for speed. However, because the temporal

resolution of the voltage measurement provided information about the physical aspects of DEP, the two pieces of "realtime" software were highly optimized for speed.

A.2   Modeling Code

- DEP_equations is a Maple worksheet in which we derived some of the equations governing the DEP fields and their consequent force, discussed in section 4.3.1.

- Kirchoff is a Maple worksheet that solves Kirchoff's Loop and Junction laws for the trap voltage in our lumped element analysis model, using the circuit in figure 4.4.

- Sliding Curves is a Mathematica notebook that allows prediction of the number of CNTs using the voltage equations from Kirchoff.

- Comsol Multiphysics model files are included in a zip package available for download.

- CNT_diffusion_spherical is a Matlab script that solves the diffusion equation in spherical coordinates. While not used in this work, it provides a visual representation for how fast diffusion occurs on the relevant length scales in our geometries.
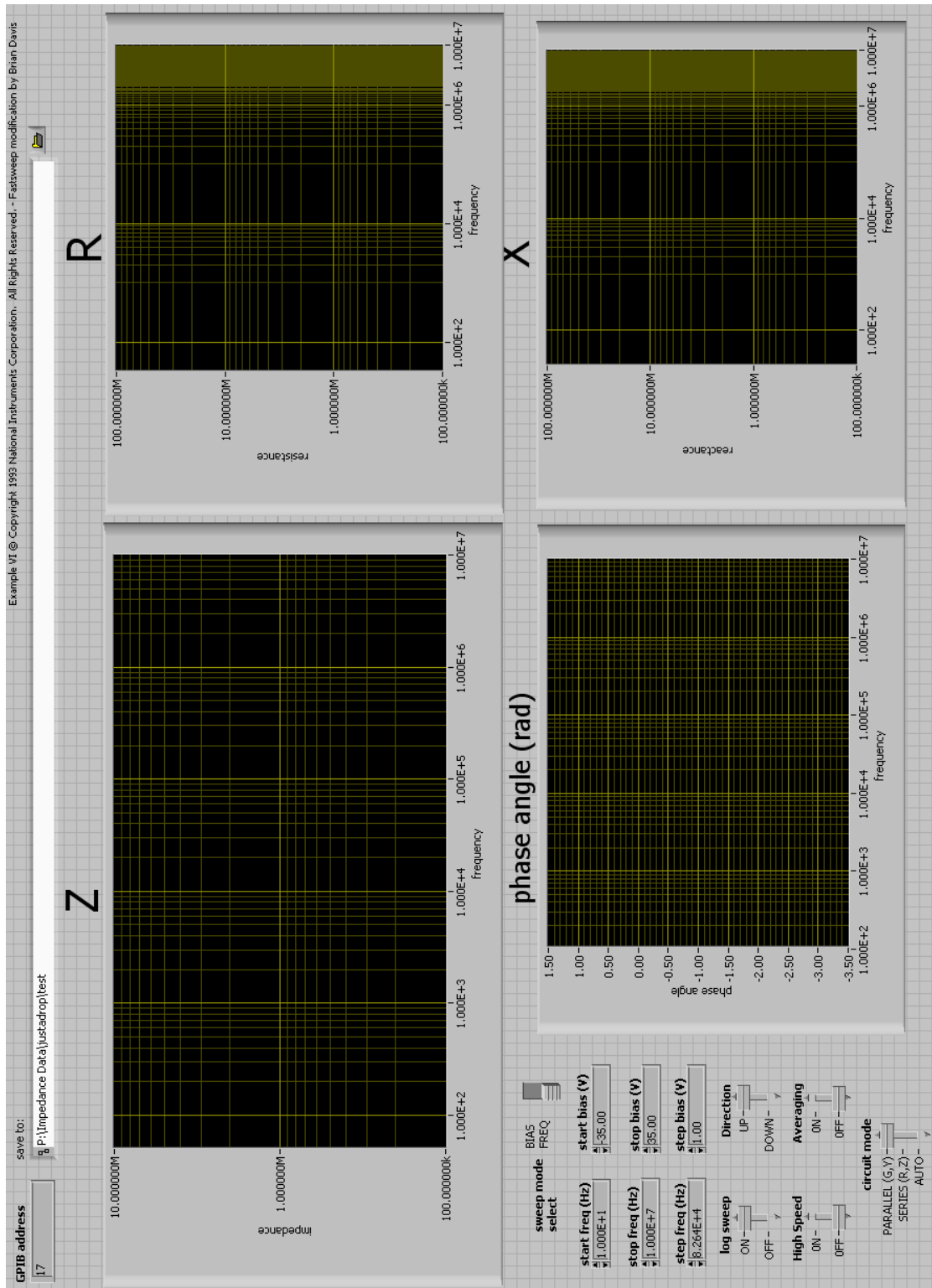
Figure A.1 The front panel setup for running Fastsweep. This program allows you to control impedance or voltage sweeps taken using the HP4192 with a variety of options.
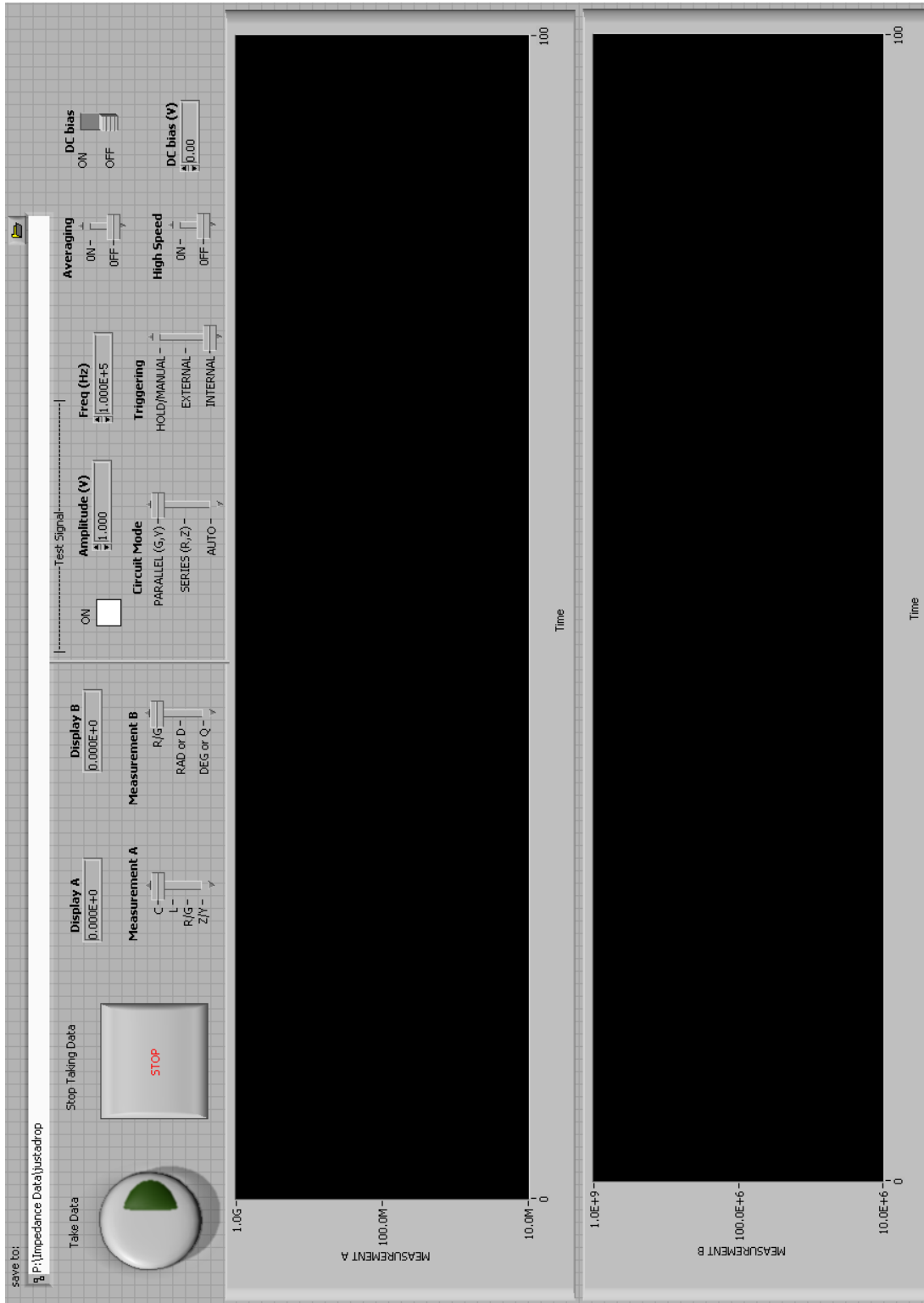
Figure A.2 This program plots data taken with the impedance spectrometer as a function of time and saves it to a spreadsheet.
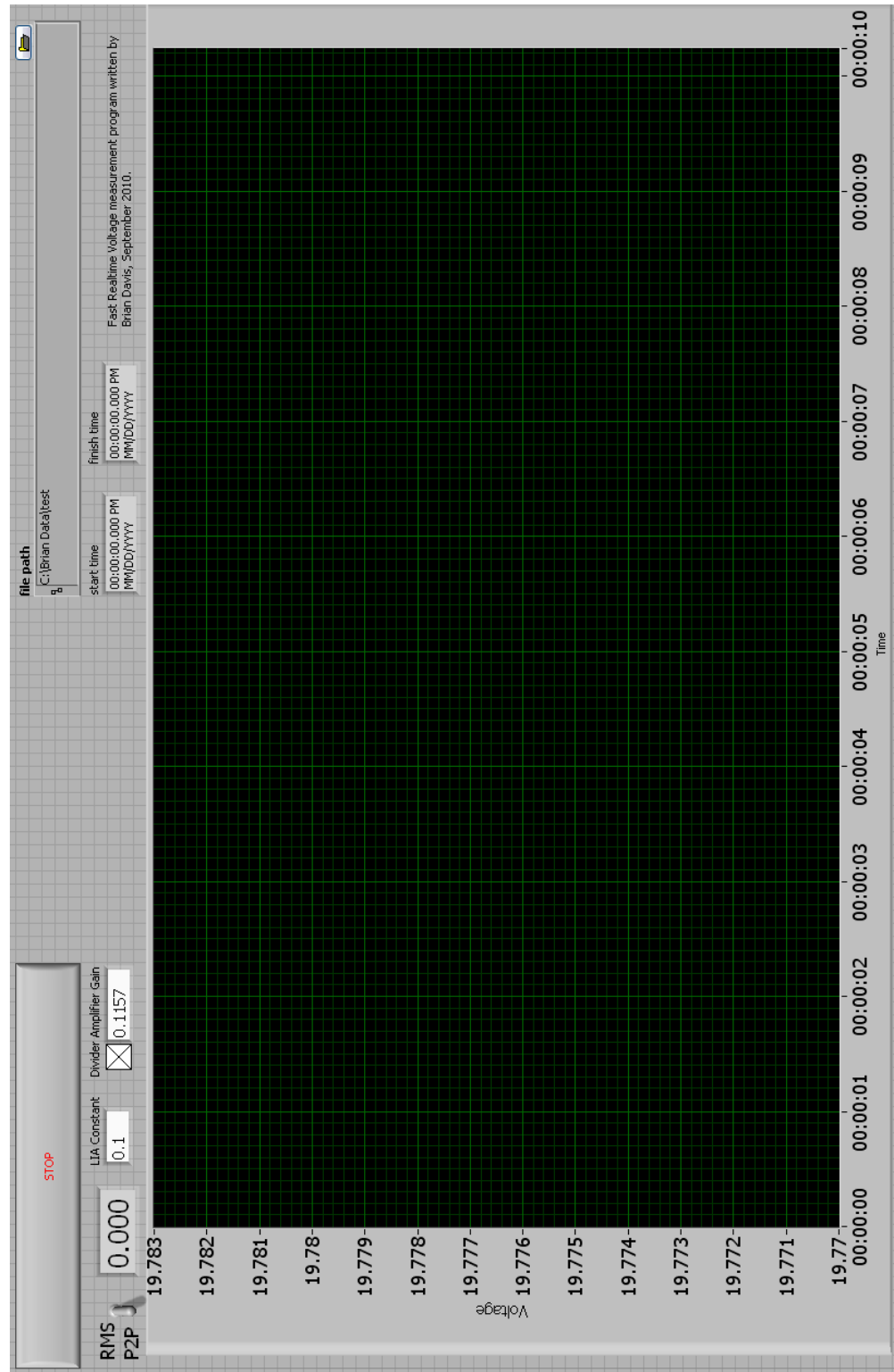
Figure A.3 This program plots data taken with the voltage measuring circuit of figure 2.8 via the lock-in amplifier feed into the NI-DAQ card. The signal is scaled by a calibration factor to compensate for the gain of the meter.
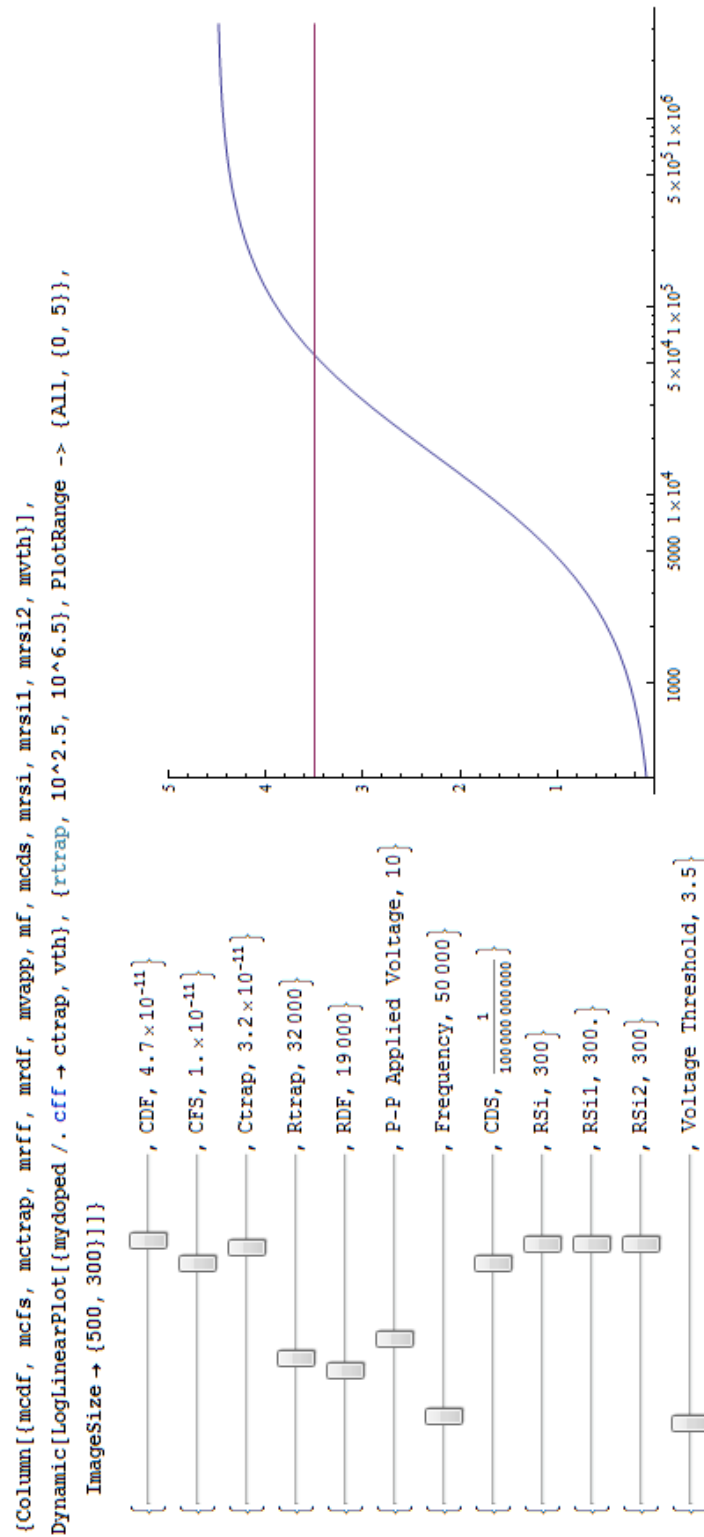
Figure A.4 Mathematica's capability of manipulating variables real-time was used to determine how the various lumped parameters changed the trap voltage.

Bibliography

[1] S. Iijima *et al.*, "Helical microtubules of graphitic carbon," Nature **354,** 56–58 (1991).

[2] M. Jose-Yacaman, M. Miki-Yoshida, L. Rendon, and J. Santiesteban, "Catalytic growth of carbon microtubules with fullerene structure," Applied physics letters **62,** 202–204 (2009).

[3] T. Guo, P. Nikolaev, A. Rinzler, D. Tománek, D. Colbert, and R. Smalley, "Self-assembly of tubular fullerenes," The Journal of Physical Chemistry **99,** 10694–10697 (1995).

[4] J. Mintmire, B. Dunlap, and C. White, "Are fullerene tubules metallic?," Physical Review Letters **68,** 631–634 (1992).

[5] J. Wildoer, L. Venema, A. Rinzler, R. Smalley, and C. Dekker, "Electronic structure of atomically resolved carbon nanotubes," Nature **391,** 59–62 (1998).

[6] T. Odom, J. Huang, P. Kim, and C. Lieber, "Atomic structure and electronic properties of single-walled carbon nanotubes," Nature **391,** 62–64 (1998).

[7] T. Durkop, S. Getty, E. Cobas, and M. Fuhrer, "Extraordinary mobility in semiconducting carbon nanotubes," Nano Letters **4,** 35–39 (2004).

[8] Z.-B. Zhang, X.-J. Liu, E. E. B. Campbell, and S.-L. Zhang, "Alternating current dielectrophoresis of carbon nanotubes," Journal of Applied Physics **98,** 056103 (2005).

[9] S. J. Tans, A. R. M. Verschueren, and C. Dekker, "Room-temperature transistor based on a single carbon nanotube," Nature **393,** 49–52 (1998).

[10] A. Bachtold, P. Hadley, T. Nakanishi, and C. Dekker, "Logic Circuits with Carbon Nanotube Transistors," Science **294,** 1317–1320 (2001).

[11] V. Derycke, R. Martel, J. Appenzeller, and P. Avouris, "Carbon Nanotube Inter- and Intramolecular Logic Gates," Nano Letters **1,** 453–456 (2001).

[12] A. Modi, N. Koratkar, E. Lass, B. Wei, and P. Ajayan, "Miniaturized gas ionization sensors using carbon nanotubes," Nature **424,** 171–174 (2003).

[13] C. Kocabas, H. sik Kim, T. Banks, J. A. Rogers, A. A. Pesetski, J. E. Baumgardner, S. V. Krishnaswamy, and H. Zhang, "Radio frequency analog electronics based on carbon nanotube transistors," Procedings of the National Academy of the Sciences **105,** 1405–1409 (2008).

[14] P. McEuen, "Single-wall carbon nanotubes," Physics World **13,** 31–36 (2000).

[15] G. students complaining in the Basement, "I hate my life," Slavery **999,** 1–10 (1800-2011).

[16] J. Kong, H. Soh, A. Cassell, C. Quate, and H. Dai, "Synthesis of individual single-walled carbon nanotubes on patterned silicon wafers," Nature **395,** 878–881 (1998).

[17] H. A. Pohl, "The Motion and Precipitation of Suspensiods in Divergent Electric Fields," Journal of Applied Physics **22,** 869–871 (1951).

[18] K. Yamamoto, S. Akita, and Y. Nakayama, "Orientation and purification of carbon nanotubes using ac electrophoresis," Journal of Physics D: Applied Physics **31,** L34–L36 (1998).

[19] M. S. Arnold, A. A. Green, J. F. Hulvat, S. I. Stupp, and M. C. Hersam, "Sorting carbon nanotubes by electronic structure using density differentiation," Nature **1,** 60–65 (2006).

[20] X. Tu, S. Manohar, A. Jagota, and M. Zheng, "DNA sequence motifs for structure-specific recognition and separation of carbon nanotubes," Nature **460,** 250–253 (2009).

[21] M. R. Diehl, S. N. Yaliraki, R. A. Beckman, M. Barahona, and J. R. Heath, "Self-Assembled, Deterministic Carbon Nanotube Wiring Networks," Angew. Chem. Int. Ed. **41,** 353–356 (2002).

[22] G. F. Close, S. Yasuda, B. Paul, S. Fujita, and H.-S. P. Wong, "A 1 GHz Integrated Circuit with Carbon Nanotube Interconnects and Silicon Transistors," NanoLetters **8,** 706–709 (2008).

[23] J. Chung, K. Lee, J. Lee, and R. Ruoff, "Toward large-scale integration of carbon nanotubes," Langmuir **20,** 3011–3017 (2004).

[24] A. Vijayaraghavan, S. Blatt, D. Weissenberger, M. Oron-Carl, F. Hennrich, D. Gerthsen, H. Hahn, and R. Krupke, "Ultra-Large-Scale Directed Assembly of Single-Walled Carbon Nanotube Devices," NanoLetters **6,** 1556–1560 (2007).

[25] L. A. Nagahara, I. Amlani, J. Lewenstein, and R. K. Tsui, "Directed placement of suspended carbon nanotubes for nanometer-scale assembly," Applied Physics Letters **80,** 3826–3828 (2002).

[26] R. Krupke, F. Hennrich, M. Kappes, and H. Lohneysen, "Surface conductance induced dielectrophoresis of semiconducting single-walled carbon nanotubes," Nano Letters **4,** 1395–1400 (2004).

[27] L. Dong, V. Chirayos, J. Bush, J. Jiao, V. M. Dubin, R. V. Chebian, Y. Ono, J. John F. Conley, and B. D. Ulrich, "Floating-Potential Dielectrophoresis-Controlled Fabrication of Single-Carbon-Nanotube Transistors and Their Electrical Properties," J. Phys. Chem. B **109,** 13148–13153 (2005).

[28] S. Banerjee, B. E. White, L. Huang, B. J. Rego, S. Oï£¡Brien, and I. P. Hermana, "Precise positioning of single-walled carbon nanotubes by ac dielectrophoresis," J. Vac. Sci. Technol. B **24,** 3173–3178 (2006).

[29] R. Krupke, F. Hennrich, H. Weber, D. Beckmann, O. Hampe, S. Malik, M. Kappes, and H. v. Lohneysen, "Contacting single bundles of carbon nanotubes with alternating electric fields," Applied Physics A: Materials Science & Processing **76,** 397–400 (2003).

[30] R. Krupke, F. Hennrich, H. Weber, M. Kappes, and H. Lohneysens, "Simultaneous deposition of metallic bundles of single-walled carbon nanotubes using ac-dielectrophoresis," Nano Letters **3,** 1019–1023 (2003).

[31] Y. Xu, A. Barnard, and P. McEuen, "Bending and Twisting of Suspended Single-Walled Carbon Nanotubes in Solution," Nano letters **9,** 1609–1614 (2009).

[32] A. Arun, P. Salet, and A. Ionescu, "A Study of Deterministic Positioning of Carbon Nanotubes by Dielectrophoresis," Journal of Electronic Materials **38,** 742–749 (2009).